Autonomous Industrial IoT for Civil Engineering Structural Health Monitoring

Gaël Loubet, *Member, IEEE*, Alassane Sidibe, *Member, IEEE*, Philippe Herail, Alexandru Takacs, *Member, IEEE*, and Daniela Dragomirescu, *Senior Member, IEEE*

***Abstract*—This article presents a wireless sensing node (SN) part of a wireless sensor network (WSN) dedicated to the deployment of a cyber–physical system intended for the Structural Health Monitoring of reinforced concretes. This low-power SN requires less than 21 mJ for a full processing: measurement, data formatting, and transmission of a 17-bytes LoRaWAN frame; *id est* 39 μJ per transmitted bit. It is designed to be buried in reinforced concrete and is battery-free and energy autonomous for long-term deployment by a radiative electromagnetic wireless power transfer (WPT) approach. The SN is cold-start compatible down to a power of –17 dBm available at the output of the antenna. It is able to wirelessly transmit data over at least tens of meters thanks to the LoRaWAN wireless communication technology. Moreover, it is wirelessly, remotely, and omnidirectionally powered and controlled by a communicating node (CN) over meters, with the respect of regional regulatory constraints (equivalent isotropic radiated power (EIRP) of +33 dBm allowed in the 868-MHz industrial, scientific and medical (ISM) frequency band). By being a generic platform, this SN can employ various sensors to measure relevant parameters for the targeted application, *id est*: temperature, relative humidity, mechanical deformation through the strain, and electrical resistivity whose the variation allows to estimate the corrosion rate. By simultaneously using the same 868-MHz ISM frequency band for the wireless communication and the WPT, the SN meets the simultaneous wireless information and power transfer paradigm with a unique antenna and without interferences. Thus, the tested system allows the deployment of the subnetwork of two CNs and several SNs (currently four) to cover a surface/volume of several meters, currently up to 11 m around each CN indoors. Finally, this system can be easily deployed for other applications requiring energy autonomous WSNs, especially in harsh environments, such as reinforced concretes, space, underground mining, power plants, etc.**

***Index Terms*—Cyber–physical system (CPS), Industrial Internet of Things (IIoT), nondestructive testing (NDT), simultaneous wireless information and power transfer (SWIPT), structural health monitoring (SHM), wireless communications, wireless power transfer (WPT), wireless sensor network (WSN).**

Manuscript received 22 May 2023; revised 13 September 2023; accepted 27 September 2023. Date of publication 3 October 2023; date of current version 21 February 2024. This work was supported in part by the French National Research Agency (ANR) under the McBIM Project (Communicating Material at the Disposal of the Building Information Modeling) under Grant ANR-17-CE10-0014, and in part by the Région Occitanie under the OPTENLOC Project. *(Corresponding authors: Gaël Loubet; Daniela Dragomirescu.)*

Gaël Loubet and Daniela Dragomirescu are with LAAS-CNRS, Université de Toulouse, CNRS, INSA, 31400 Toulouse, France (e-mail: gael.loubet@laas.fr; daniela.dragomirescu@laas.fr).

Alassane Sidibe is with LAAS-CNRS, Université de Toulouse, CNRS, UWINLOC, 31400 Toulouse, France (e-mail: alassane.sidibe@laas.fr).

Philippe Herail is with LAAS-CNRS, Université de Toulouse, CNRS, 31400 Toulouse, France (e-mail: philippe.herail@laas.fr).

Alexandru Takacs is with LAAS-CNRS, Université de Toulouse, CNRS, UPS, 31400 Toulouse, France (e-mail: alexandru.takacs@laas.fr).

Digital Object Identifier 10.1109/JIOT.2023.3321958

I. Introduction

In recent decades, the digitalization and miniaturization of electronics have led to a huge increase in the use of embedded electronic systems. The main objective is to have more functionalities on less volume and less power consumed. In this trend, wireless communications have played a key role by allowing moving remote and wireless communications between humans and/or machines. Thus, the machine-to-machine (M2M) wireless communications have made possible the development of wireless sensor networks (WSNs) [1]. The latter can be employed to monitor and/or control the physical world, as well as to connect the physical and digital worlds, in what is called cyber–physical systems (CPSs) [2]. Moreover, these WSNs are the basic building block of the Internet of Things (IoT) paradigm which aims to make the communicating devices ubiquitous [3].

No matter the targeted application, the long-term deployment of WSNs is currently severely limited by their energy autonomy. A large part of the deployed WSNs is based on the use of batteries (primary or secondary) as of right now. These have a restricted lifetime and their manual replacement is time consuming and expensive. To ensure the long-term energy autonomy of WSNs, ambient energy harvesting and wireless power transfer (WPT) solutions are investigated [4]. The ambient energy harvesting solutions are based on the scavenging of residual energy available in the environment. These energies can be light, mechanical/kinetic, thermal or electromagnetic. Nevertheless, these are highly dependent on the environment of deployment, fluctuating, unpredictable and uncontrollable. To overcome these limitations, a power source is used in WPT solutions to make the scavenging of the specifically provided energy controllable, predictable, low fluctuating, and low dependent on the environment of deployment. Currently, the WPT solutions employ light, mechanical/kinetic and electromagnetic powers.

Regarding the electromagnetic WPT, several technologies coexists: in near-field (capacitive, nonresonant inductive and resonant inductive) and in far-field (radiative) [5]. Despite their high efficiencies and large variety of performances, near-field solutions have generally a short range of use (from millimeters to a few meters), which makes these unsuitable for WSNs deployed in broad areas (e.g., from rooms, to cities, through

buildings) unlike far-field solutions. These last provide various performances usually dependent of the targeted application and of the regional regulations (both in terms of frequency bands and maximum EIRP allowed) [6] and achieve a range of use of at least several meters. By considering both the wireless communication and the radiative electromagnetic WPT, some WSNs meet the simultaneous wireless information and power transfer (SWIPT) paradigm [7].

At the same time, structural health monitoring (SHM) is becoming increasingly common in all application fields [8]. It consists in continuously overseeing the state of health of a thing, to prevent its irreversible failures, avoid its collapse, and allow to apply preventive treatments. To achieve it, nondestructive testing (NDT) methods are privileged because these do not alter the element under test [9], [10], [11]. Also, the use of digital twins (such as a building information modeling (BIM) in the civil engineering industry [12]) can be a relevant way to keep up-to-date a model of the element. The current and past information of these elements would be easily accessible for the different stakeholders (owners, users, etc.). Thus, CPSs based on WSNs are suitable for the implementation of autonomous SHM applications in various fields.

Furthermore, the "communicating material" paradigm has been established [13]. This defines materials that are full CPSs dedicated to SHM applications in various fields. These are intrinsically able to: 1) measure (with NDT methods); 2) process (locally and/or remotely); 3) store (locally and/or remotely); and 4) share (locally—with other communicating materials, WSNs, or wireless communicating devices—and/or remotely—especially with digital twins located in the digital world, through the Internet-) data characterizing their own internal health and/or their environment. This allows to have an updated follow-up of the materials and the structures to which these belong, during all their lifetime (from their manufacturing to their recycling, through their construction and exploitation). It also provides access to a history of the materials and the structures that is always accessible to authorized humans and/or machines.

In this context, the material communicating with the BIM (McBIM) project, funded by the French National Research Agency (ANR), deals with the design and implementation of a communicating material for the civil engineering industry: a communicating reinforced concrete [14], [15]. This is a full Industrial IoT (IIoT) system dedicated to SHM of reinforced concretes and civil engineering structures. It is based on an energy autonomous WSN embedded in the material and able to update during all its life a BIM available through the Internet. Due to a need for genericity (to be independent of the targeted environment and application) and due to the inaccessibility of the system once deployed in the material, a battery-free WSN wirelessly powered by radiated electromagnetic waves has been chosen [16], [17], [18].

Thus, this article focuses on the design, the implementation, and the test of energy autonomous sensing nodes (SN), fully buried in reinforced concrete and part of a WSN. These are battery-free, wirelessly and remotely powered and controlled, and capable of measuring and wirelessly transmitting relevant data for the SHM of reinforced concretes. These communicate data over kilometers thanks to the LoRaWAN wireless communication technology and are wirelessly powered over several meters (at least up to 11 m) in all the directions from a power source respecting the European regulations. By using simultaneously the 868-MHz industrial, scientific, and medical (ISM) frequency band for both the wireless communication and the WPT, the proposed SNs meet the SWIPT paradigm with a unique antenna.

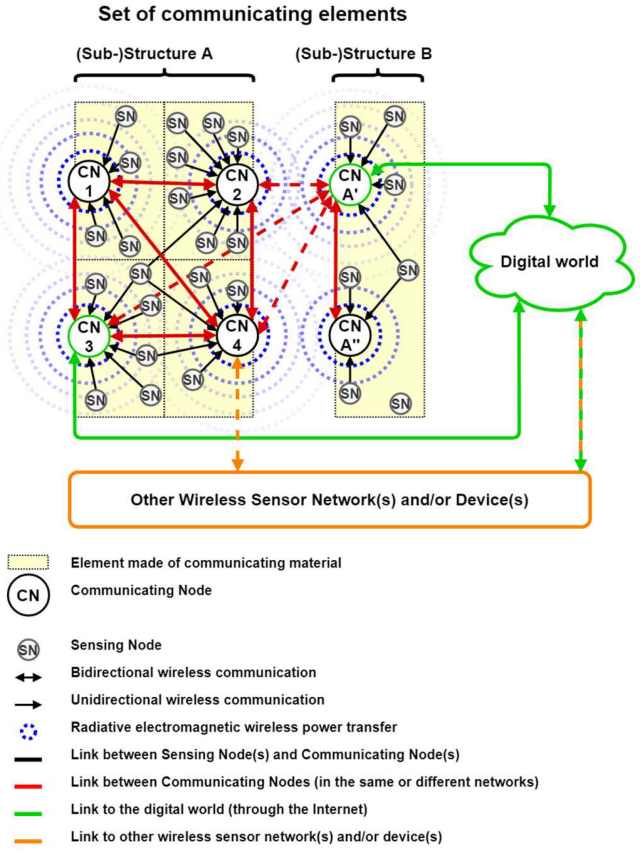

Fig. 1. Block diagram of the architecture of the CPS dedicated to the implementation of communicating materials.

Section II will address the designs of the CPS, and more specifically of the SNs, by considering the current State of the Art in the various areas. Section III will deal with the characterization and test of the SNs, and how the power consumption has been significantly reduced. Before concluding, Section IV will propose the analysis of the presented results, as well as will provide some axes of improvement and some future axes of research.

II. Architectures of the Cyber–Physical System and of the Sensing Nodes

A. Cyber–Physical System

The global architecture of the proposed CPS is presented in Fig. 1 [16], [17], [18]. Even though it was imagined for a communicating reinforced concrete, this CPS can be easily scalable to other communicating materials, as well as other SHM applications, especially in harsh environments. Its physical part is

a WSN composed of two kinds of node, organized in a two-levels network. There are the communicating nodes (CNs) and the SNs. Each element made of communicating material embeds at least one CN and several SNs, this association forming a subnetwork. Their number is a function of the size of the element and the needs in terms of measurement (especially in terms of spatial precision).

The CNs form an *ad-hoc* meshed network within a structure or a set of adjacent structures. These are intended to aggregate the data transmitted by the SNs, then process, store, and share it. The data can be processed, stored and shared locally in one or more CNs of the network, and/or remotely in one or more other networks, in one or more other devices, or even in the digital world, and in particular in a digital twin, thanks to an access to the Internet. Thus, bidirectional medium to long-range wireless communication technologies are required between the CNs. Moreover, at least one CN per meshed network must be a reliable access point (or a gateway) to the digital world by providing a bidirectional connection to the Internet. Other bidirectional wireless communications technologies can be implemented to interface with other WSNs and/or devices.

A star network of SNs is available around each CN, thus, it becomes a central hub in a subnetwork. The SNs are intended to measure relevant parameters of the monitored element and/or its environment. The collected data must then be transmitted to the associated CN(s) with directional medium range wireless communication technologies. In addition to the recovery of the data sent by the SNs, the CNs must wirelessly power the SNs located in their neighborhood. By tuning their wireless power source (in terms of waveform, output power and/or periodicity of activation), the CNs can set up the periodicity of functioning of the SNs. A radiative electromagnetic WPT system is used to achieve this aim.

For the communicating reinforced concrete, a major part of the electromagnetic propagation medium (both for the wireless communication and the WPT) is composed of reinforced concrete, which is highly constraining to the electromagnetic waves [19].

B. Communicating Nodes

The CNs must achieve several functions: 1) collect the data sent by the SNs located in their neighborhood; 2) aggregate, process, store, and share—locally and/or remotely—the data provided by the SNs, by the other CNs, by the other WSNs and/or Devices, and/or by the digital twin(s); and 3) wirelessly power and control the SNs located in their neighborhood, thanks to a WPT system [16].

Thus, these are composed of two main subsystems: a radiative electromagnetic power source; and a control and data management and storage system, which also control the first subsystem. From another point of view, the CNs present several interfaces, which require different performances (in terms of use, of directionality, of periodicity, of range, of data rate, etc.) but which could be mutualized. These are: 1) for the collection of data from the SNs; 2) for the WPT; 3) for the communication with the other CNs; 4) for the connection with the Internet; and 5) for each other types of wireless communication employed.

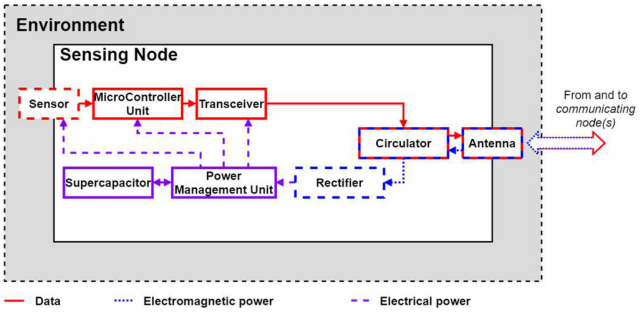

Fig. 2. Block diagram of the proposed generic architecture of the SN.

In the presented implementation, the CNs are composed of a LoRaWAN gateway [based on a Raspberry Pi 3 model B+ from the Raspberry Pi Foundation (Caldecote, Cambridgeshire, U.K.) and an iC880A LoRaWAN concentrator for IMST (Kamp-Lintfort, Germany), and using the Raspberry Pi OS Lite operating system from the Raspberry Pi Foundation (Caldecote, Cambridgeshire, U.K.), the user datagram protocol packet-forwarder from Semtech (Camarillo, CA, USA) and some Chirpstack tools (Orne Brocaar)] with Wi-Fi, Ethernet, and cellular interfaces (a Bluetooth interface is available but not used) associated with a homemade power source [designed with components from Mini-Circuits (Brooklyn, NY, USA)] providing a continuous wave (CW) signal with an EIRP of +33 dBm (or +3 dB, or 2 W) in the 868-MHz ISM frequency band [6]. More details on its implementation are available in [16].

C. Sensing Nodes

The SNs are the core elements of this CPS, because gathering the main constraints: inaccessibility (once deployed and embedded into the material), energy autonomy, fully wireless, long lifespan (that of the material itself (e.g., decades for reinforced concretes)), and so long-term usability, resilience and reliability [16], [17], [18].

1) Architecture: The architecture of the proposed SN is presented in Fig. 2. The SNs are designed as simple as possible in order to minimize the risk of failure.

The SNs must achieve one main function: sense some physical parameters to quantify the internal health state of the material and/or its environment, and wirelessly transmit the collected (and possibly preprocessed) data to the CN(s). Moreover, these must be energy autonomous for their entire lifetime and, thus, be battery-free and able to cold-start, and their periodicity of use must be controlled by the CNs.

Therefore, these are composed of two distinct subsystems which interact: one dedicated to the power management and the other to the collection and transmission of data. The power management subsystem is composed of: a harvester (a rectenna, i.e., an antenna and an RF-to-dc rectifier, here connected through a radio-frequency circulator) used to harvest the radiative electromagnetic power generated and transmitted by the CN(s) and to convert it into dc electrical power;

and a power management unit (PMU) used to efficiently recover the power provided by the rectenna, to store it in energy storage buffer (here a supercapacitor), and to power the data management subsystem once enough energy is available. The data management subsystem is composed of a microcontroller unit (MCU) which drives a sensor and a wireless transceiver (here a LoRaWAN one) connected to the same antenna as for the power management subsystem (through the radio-frequency circulator). The aim is to measure physical parameter(s), preprocess the data, and wirelessly send these to the CN(s) each time that the subsystem is powered.

Even though it could be attractive to send the raw data directly to further reduce the power consumption of the SNs, a preprocessing step is specified to propose a generic system applicable to various use-cases. Generally, the power/energy consumption during processing time is much lower than during transmitting time. The overall power consumption of the SNs can be reduced by limiting the amount of data to be sent and by minimizing the transmitting time. This may involve reducing the size of the data by reformatting or aggregating (e.g., averaging, pruning), in case of large format, or multiple data and/or data redundancy. Here, the preprocessing is just data reformatting to reduce the size of the payload.

Finally, the proposed SN is well suited for long-term deployment expressed in decades in harsh environments: 1) where maintenance is impractical because SNs are inaccessible or difficult to access (e.g., buried in material, at very high heights, in satellites, in nuclear area, etc.); 2) which are isolated and without main power (e.g., desert, forests, mountains, etc.); and 3) where batteries are unusable (e.g., explosive conditions, extreme temperatures, high humidity, radiations, dust, dirt, etc.) and ambient energy harvesting solutions unexploitable (e.g., caves, underground mining, etc.).

2) Design and Implementation:

a) Sensors: To certify standards, and mechanical or physical properties of concretes, these must be monitored on several parameters during their entire life. Even though the parameters to follow are different according to the step in the lifecycle (manufacture, curing, construction, exploitation, demolition, or recycling), some are more relevant and can be used during all the lifecycle: temperature, humidity, pH, corrosion, strain or stress, and cracks detection and location [9], [10], [11], [20]. The main objective is to warranty a safe use of the material and of the structure, particularly by checking for their proper aging, and by detecting, locating and quantifying the damages, or even predicting these. This allows to perform maintenance or even predictive maintenance, when required and before the damages become irreversible.

In order to be implementable in WSNs and to allow a continuous (with slowly evolving parameters), automatic and remote monitoring, the destructive (or semidestructive) testing methods are rejected in favor of NDT methods [9], [10], [11], [20]. Moreover, to limit the needs in terms of energy and computing capacity, the direct and temporally punctual measurement methods are privileged and the methods requiring signal processing and/or energy-consuming equipment are discarded. Also, the proposed SNs are based on a generic platform where different kinds of low-power sensors can be connected.

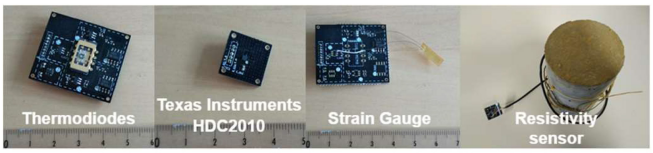

Fig. 3. Photographs of the daughter boards dedicated to the implementation of different sensors.

Currently, four different kinds of sensors have been successfully implemented and tested: 1) temperature; 2) temperature and relative humidity; 3) strain; and 4) dielectric resistivity; which are presented in Fig. 3.

The temperature, and temperature and relative humidity sensors deal with physical parameters. Considered together, these two physical parameters can be used in various applications during all the life of reinforced concretes, especially for the curing and the exploitation phases. Both academic and commercially available sensors have been used: in particular, thermodiodes from the University of Cambridge (Cambridge, U.K.) as temperature sensors [21], and HDC2010 from Texas Instruments (Dallas, TX, USA) as a temperature and relative humidity sensor [22]. These are supplied with a 3.3-V supply voltage, consume, respectively, 600 μW and 200 nW on stand-by, and present measurement ranges between -40°C and $+125$ °C with an accuracy of ± 0.2 °C (temperature) and 0%–100% with an accuracy of $\pm 2\%$ (relative humidity, if applicable).

The strain sensor deals with a mechanical parameter: the strain. This mechanical parameter can be used in various applications during all the life of reinforced concretes to estimate the mechanical deformation. A commercially available simple and low-cost wire lead strain gauge has been used as a proof-of-concept [23]. This is supplied with a 3.3-V supply voltage and consumes 1.46 mW on stand-by.

The dielectric resistivity sensor deals with a chemical parameter: the corrosion. The corrosion rate can be estimated by the study of the evolution of the dielectric resistivity over time. This chemical parameter can be used in various applications during all the life of reinforced concretes. A fully buried academic Wenner probe from the Laboratory for Materials and Durability of Constructions (LMDCs, Toulouse, France) has been used [24]. This is supplied with a 3.3-V supply voltage and consumes 580 μW on stand-by.

Although the SHM of reinforced concretes can be achieved during the major part of their lifecycle by correlating the data provided by all the implemented sensors, other kinds of sensors could be investigated [9], [10], [11], [20]. Furthermore, some improvements could be achieved in order to maximize the accuracy and/or the range, while minimizing the power consumption.

b) Microcontroller unit and wireless transceiver: To drive the sensor, and to process and transmit the data, an MCU driving a wireless transceiver must be implemented in the SNs. Indeed, these must transmit at low power the few bytes of data collected over at least a few tens of meters from inside

the material (here reinforced concrete) to the CN(s). Thus, for reasons of hardware security (fixed firmware and no access to alter or update it) and power consumption (no time dedicated to the listening of the communication medium), only the data uplink in a configuration that does not require connection or acknowledgment is used. Consequently, the SNs are not able to receive data. There are several solutions that can be employed for these wireless transmissions.

Electromagnetic wireless communications technologies [1] have been selected in contrary of those based on the light [25] or the mechanical [26], [27], [28] waves, because: these provide no commercially available solutions; and cannot be efficiently used at medium to long ranges through all the media (e.g., light in the reinforced concrete and mechanical waves in the air). Among the wide variety of technologies available, the focus has been on the wireless personal area networks (WPANs) [29] (e.g., Bluetooth (IEEE 802.15.1 [30]), Bluetooth Low Energy (IEEE 802.15.1 [30]), ZigBee (IEEE 802.15.4 [31], [32]), etc.) and the low-power wide-area networks (LPWANs) [33] (e.g., LoRaWAN [34], DASH7 (ISO 18000-7 [35]), etc.) for reasons of power consumption, data rates, availability, and range of use. For the future, and if commercially available, ultrawide band (UWB) (IEEE 802.15.3 [36], [37]), and RuBee (IEEE 1902.1 [38]) (theoretically able to reliably communicate through reinforced concretes over 10 m), as well as mechanical communications (if the reinforced concrete is the propagation medium) are relevant investigation trends.

Preliminary qualitative tests for indoor wireless communications have been performed. This enabled the LoRaWAN technology to be chosen from among three representative wireless communication technologies tested without their operation being optimized in terms of power consumption: Bluetooth Low Energy, UWB, and LoRaWAN. This choice was based on two criteria: 1) the range of use indoor, and especially the ability to pass through reinforced concrete walls and ceilings/floors, without loss of frame and 2) the power consumption in active mode. The UWB solution based on the DW1000 transceiver from Qorvo (Greensboro, NC, USA) has the shortest range (limited to a few meters) without the ability to pass through reinforced concrete, but also the highest power consumption in active mode: approximately 230 mW at 3.3 V. The Bluetooth Low-Energy solution based on the nRF52832 module from Nordic Semiconductor (Trondheim, Norway) has a range of tens of meters with the ability to pass through some reinforced concrete elements, and for the lowest power consumption in active mode: approximately 25 mW at 3.3 V for a +3-dBm transmission. The LoRaWAN solution based on the SX1272 transceiver from Semtech (Camarillo, CA, USA) has the longest range, easily exceeding a few hundreds of meters. It covers the entire LAAS-CNRS laboratory which is distributed over four levels with distances of a few hundreds of meters, and even well beyond, with the ability to pass through a lot of reinforced concrete elements without loss of frame, and for a power consumption in active mode: approximately 100 mW at 3.3 V for a +14-dBm transmission. That is, considered low but remains relatively high compared with the Bluetooth Low-Energy solution. At this stage, it appeared that a single LoRaWAN gateway was sufficient to cover more space than required, thanks to the chirp spread spectrum (CSS) technique which appears not too sensitive to the reinforced concrete.

In terms of power consumption, LoRaWAN can be considered as one of the "worst" cases among LPWAN and WPAN technologies. Therefore, the success of its implementation (with its power supply by WPT) will provide one of the worst characteristics, only improvable, and will certify the possibility to use technologies requiring less energy. For this reason, some experimentations with Bluetooth Low Energy have already been successfully carried out with similar SNs [39].

Because compact, inexpensive and complete, an all-in-one CMWX1ZZABZ-091 LoRaWAN module from Murata (Nagaokakyōshi, Kyoto, Japan) [40] (based on an SX1276 LoRa transceiver from Semtech (Camarillo, CA, USA) [41] and an STM32L072CZ microcontroller from STMicroelectronics (Amsterdam, The Netherlands) [42]) requiring a 3.3-V voltage supply has been used. Nevertheless, solutions based on independent MCU and LoRa transceiver could allow a wider design flexibility at the price of a more complex system. To provide a generic platform, all the interfaces are made available for the connection of all kinds of sensors. The firmware developed in C and employing the LoRaWAN stack provided by Semtech (Camarillo, CA, USA) is reduced to a one-shot measurement and a LoRaWAN transmission. This measurement process starts with the initialization of the MCU, interfaces, and desired peripherals; followed by the control of the sensor to obtain the measurement. Preprocessing of the data to format it as a 2-byte integer to get a generic and reduced data format regardless the kind of measurement, in particular to facilitate interfacing with partners is then performed. Before going into a deep-sleep mode, the formatted data is transmitted in a LoRaWAN frame. The all measurement and transmission process is depicted in Fig. 4. The LoRaWAN frames are 17-bytes long, whose 13 bytes dedicated to the LoRaWAN protocol and 4 bytes dedicated to the data payload. The payload can be reduced by optimizing the data formatting. A unique antenna is used both for the wireless communication and WPT *via* an RF circulator, and will be presented later.

c) Strategy of use: Because the targeted periodicity of measurement is long (e.g., once an hour, once a day, once a week, or once a month for the SHM of reinforced concretes depending on the phase in the lifecycle) and considering that the available electromagnetic power is largely inferior to the dc electrical power required by the data management subsystem [43], [44], a "store then use" strategy is applied. In this strategy, the scavenged power is stored, and once enough energy is available, this is used to power the data management subsystem, as presented in Fig. 4. That way, the periodicity is not controlled by the software (e.g., with events or timer interruptions) but by the hardware *via* the power management subsystem. Thus, to design the power management part of the SNs, it is necessary to know the energy these require to work properly. In any case, the minimization of the energy needed to operate the system is targeted, and can be achieved in both software and hardware.

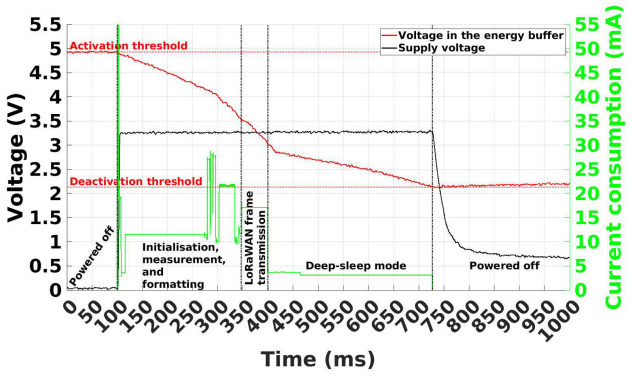

Fig. 4. Example of the power consumption of the SNs according to the phase of operation.

d) Implementation of the wireless power transfer: To be controllable, predictable, low fluctuating, and low dependent on the environment of deployment, a WPT solution is favored over ambient energy harvesting solutions, as presented in Fig. 5. For the same reasons as for wireless communications, the electromagnetic WPT is favored over light (laser or infrared) and mechanical/kinetic (sonic and ultrasonic) WPT solutions. Moreover, to achieve sufficiently wide ranges of use, near-field (capacitive, nonresonant inductive, and resonant inductive) solutions are discarded in favor of far-field (radiative) solutions. Today, the radiative electromagnetic WPT systems are oriented toward ubiquitous applications with very low-power densities. This is partly because, on the one hand, there is a desire to reduce the global energy consumption, and on the other hand, it is to ensure the safety of living beings.

The range of use of the radiative electromagnetic WPT is highly constrained by the choice of the frequency band, which is subject to regional regulations [6], and which is here chosen among the ISM radio-frequency bands. First, the free-space path losses (1) are function of the frequency: the higher the frequency, the larger the free-space losses, and the shorter the range of use. Second, the range of use (2) is a function of the transmitted power, whose maximum EIRP dependents on regional regulations

$$\text{free\_space\_path\_losses} = 20 \cdot \log\left(\frac{4 \cdot \pi \cdot d \cdot f}{c}\right) \text{(dB)} \quad (1)$$

$$\text{range} = \sqrt{\frac{\lambda^2}{4 \cdot \pi} \cdot \frac{P_{\text{EIRP}}}{3600 \cdot \pi \cdot P_{\text{IN}}}} \text{(m)} \quad (2)$$

with d the distance, f the frequency, c the celerity of light, λ the wavelength, P_{EIRP} the maximal EIRP (fixed by the regional regulations) and P_{IN} the minimum required input power.

According to Table I, which compares the use of different ISM frequency bands for the radiative electromagnetic WPT, the most attractive frequency band, with the highest range of use for a defined input power (over meters), is the 868-MHz frequency band.

The power harvester for the electromagnetic waves is a rectenna, that says an antenna connected to an RF-to-dc rectifier. Its role is to efficiently harvest the radiative electromagnetic power generated by the CNs (with a power density as low as possible); in order to provide a sufficient dc electrical power to allow the PMU and the energy buffer to efficiently and sufficiently store the energy; to finally use it to power the data management subsystem. This must be well designed to meet the properties of the transmitted power (e.g., power density level, central frequency, frequency band, polarization, etc.).

TABLE I
COMPARISON OF ISM FREQUENCY BANDS FOR THE DESIGN OF THE RADIATIVE ELECTROMAGNETIC WPT SYSTEM

Central frequency (MHz)	13.56	433	868	2,450	5,800
Wavelength in the air (cm)	2.210	69.2	34.4	12.2	5.2
Bandwidth (MHz)	0.014	1.74	5	100	150
Maximum EIRP [6] (dBm / mW)	N/A	+10 / 10	+33 / 2,000	+20 / 100	+23 / 200 or +30 / 1,000
Free-space losses at 1 m (dB)	N/A	25.17	31.21	40.23	47.71
Theoretical range for obtaining P_{IN} = +0 dBm (or 1 mW) at the output of a 0 dBi antenna for a power source generating a signal with maximum EIRP (cm)	N/A	17	123	9	6 or 13
Theoretical range for obtaining P_{IN} = -14 dBm (or 39.8 µW) at the output of a 0 dBi antenna for a power source generating a signal with maximum EIRP (cm)	N/A	87	615	48	29 or 65
Theoretical range for obtaining P_{IN} = -17 dBm (or 20.0 µW) at the output of a 0 dBi antenna for a power source generating a signal with maximum EIRP (cm)	N/A	123	869	68	41 or 92

It must be noted that the overall size of the SNs is correlated to the size of their antenna(s), which is closely related to their wavelength/frequency: the higher the frequency, the smaller the antenna; and its bandwidth: the wider the bandwidth, the larger the antenna. Thus, the choice of the frequency band must also be a tradeoff between the size of the SNs *via* the size of the antenna(s) and the range of use. At 868 MHz, the size of the antenna stays usually small enough.

In order to reduce the overall size of the SNs and because the same frequency band is used for both the wireless data communication and the WPT, it has been chosen to employ a unique antenna for the two functions. As there is only data uplink and power downlink, it has been possible to use a radio-frequency circulator C11-1FFF/OPT.N from Aerotek (Hanover, MD, USA) [45], with low insertion losses and high isolation. This way, the power harvested by the antenna is transmitted to the rectifier through the radio-frequency

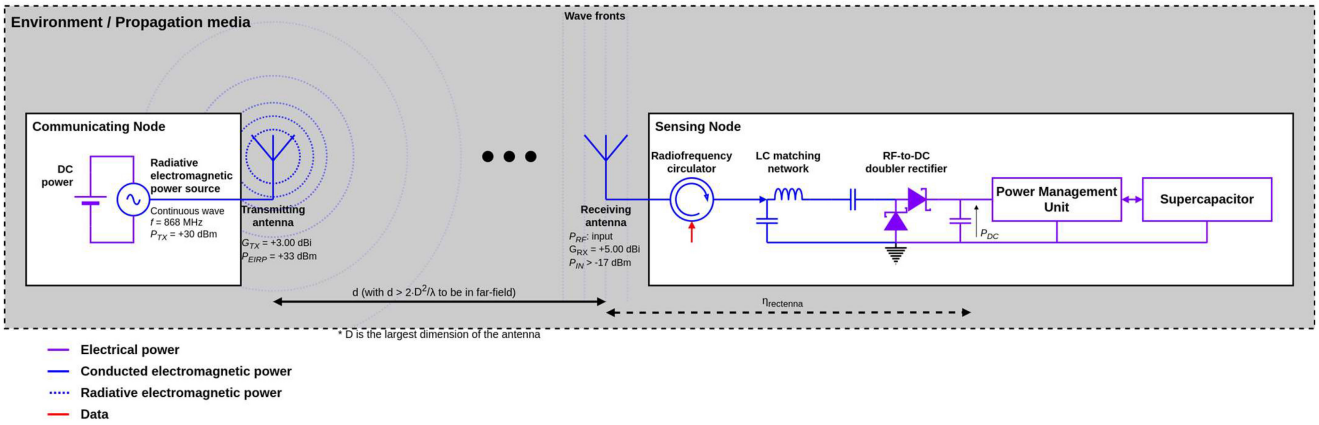

Fig. 5. Block diagram of the implementation of the WPT solution.

circulator, and the data frame provided by the transceiver is transmitted to the antenna through the radio-frequency circulator simultaneously. In addition, there is no interconnection between the rectifier and the transceiver, and no interference between the data transfer and the power transfer.

The CNs generate a narrow-band (NB) CW at a frequency close to 868 MHz *via* their radiative electromagnetic power source. The SNs and the CNs use LoRa signal based on CSS technique on one of the five defined subchannels in the 868-MHz ISM frequency band. On the SNs side, the received input signal for the WPT has a lower power level than the output one used for the data transmission. Thus, the output signal is not altered whatever the waveform of the input signal. Moreover, this behavior is further enhanced by the high isolation of the radio-frequency circulator between the output and input channels. So, there is no interference for the SNs. On the CNs side, the output signal for the WPT is considered as noise by the LoRaWAN input frame receiver. There is also no interference thanks to the noise resistance of the CSS technique.

Thus, a new solution and implementation of the SWIPT paradigm is provided, without temporal, frequential, or spatial multiplexing, neither power splitting, but with a discrimination/separation through the circulator of the sense of signal flows (data from the transceiver to the antenna and power from the antenna to the rectifier).

It must be noted that this solution does not increase the power consumption, for either the SNs or the CNs, even in case of interferences. Indeed, the SNs implement no data downlink; thus, cannot receive acknowledgment frames. In that way, no retransmission strategy is deployed, so, no increase in the power consumption can occur in case of interferences. The case of the loss of data (which eventually could be problematic) could be neglected thanks to spatial redundancy if enough SNs are deployed. Finally, as long as the CNs consider the WPT signal as noise, there is no alteration of their nominal functioning; so, no increase in their power consumption.

The antenna must meet the best tradeoff between its volume and its performances (radiation pattern, gain, polarization, etc.). The objective is to get SNs as compact as possible, with the largest possible range of use for its wireless power supply, and whose functioning is as independent as possible from their location and orientation. In consequence, the ideal antenna must be compact, have a high gain and an isotropic/omnidirectional radiation pattern.

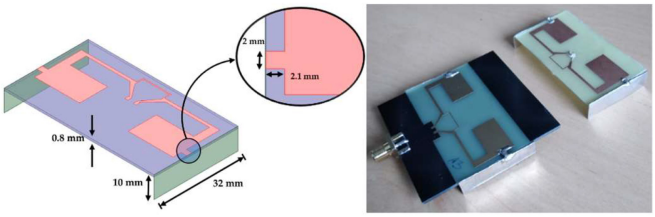

Fig. 6. Diagram and photograph of the designed and implemented printed folded quart-wavelength dipole antenna with capacitive arms at 868 MHz, on a 1.6-mm (black) and 0.8-mm (yellow) FR4 substrate.

Thus, a printed folded quart-wavelength dipole antenna with capacitive arms has been chosen, as presented in Fig. 6 [46]. This has been designed on an FR4 substrates (thickness: 0.8 and 1.6 mm; relative permittivity: 4.4; and loss tangent: 0.02) and measures 5.6 cm × 3.2 cm × 1.0 cm. A folded quarter-wavelength dipole antenna with a short-circuited loop, to make a T-match structure, is used as a base, which allows an input impedance matching to 50 Ω, and an NB and almost isotropic behavior. Metallic arms, orthogonal to the plane of the folded quarter-wavelength dipole antenna, are connected to each monopole which induces a capacitive coupling allowing to reduce the size of the antenna at the targeted frequency. This antenna is almost omnidirectional, has a linear polarization, is usable (i.e., impedance matched) between 848 and 886 MHz, has a measured gain of +1.54 dBi at 868 MHz and has a measured −3-dB beamwidth of 110° in the E-plane, as represented in Fig. 7. By adding an 8 cm × 6 cm metallic reflector plane at 5 cm from it, the measured gain is increased up to +5.00 dBi at the cost of the increase of the directionality and the rise of the volume. The measured −3-dB beamwidth is then 70° in the E-plane. In addition, the first designs of this antenna on a flexible substrate (Kapton) have been completed and have provided encouraging preliminary results.

Concerning the targeted application, the antenna must properly work in a particular environment: the reinforced concretes. It must be noted that the antenna has been successfully tested

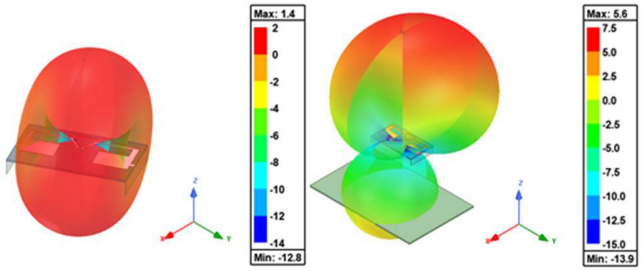

Fig. 7. Simulated (HFSS) radiation patterns of the printed folded quart-wavelength dipole antenna with capacitive arms at 868 MHz, with and without the use of a 6 cm × 8 cm metallic reflector plane located at 5 cm below the antenna/rectenna.

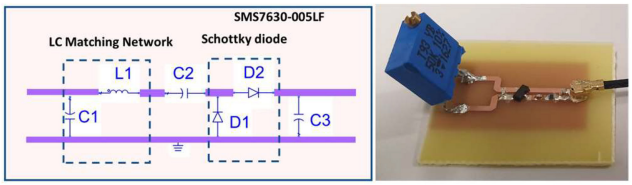

Fig. 8. Schematics and photograph of the designed and implemented full-wave rectifier on 0.8-mm thick FR4 substrate connected to a 10-kΩ load.

into a reinforced concrete beam, both for WPT and wireless communication. Nevertheless, this was not in direct contact with the reinforced concrete but located in an air cavity. It is very probable that an impedance mismatch occurs when the antenna will be directly buried into the reinforced concrete, and a redesign must be provided by considering the reinforced concrete as the main propagation medium (thus, by considering its dielectric properties which may change during time). There are in the literature some works dealing with the study, the design, the manufacturing, and the test of antenna buried into concretes [47], [48], [49], [50], [51], [52].

The rectifier must meet the best tradeoff between its efficiency, its characteristics (frequency/bandwidth, input impedance, typical range of available radio-frequency input powers, etc.) and its complexity (topology, size, nonlinear rectifying component, etc.). The objective is to get a rectifier as efficient as possible especially for the lowest power densities, and provide a sufficient voltage to the PMU for optimum operation, both in the cold-start and in the normal charging modes. Also, the rectifier must be impedance matched with the associated antenna in the targeted frequency band and must be followed by a low-pass filter in order to provide a dc voltage with a minimized ripple at the input of the PMU.

Therefore, a full-wave rectifier has been chosen, as presented in Fig. 8 [53]. This has been designed on an FR4 substrate (thickness: 0.8 and 1.6 mm; relative permittivity: 4.4; and loss tangent: 0.02) and optimized to be the most efficient for an input power of −15 dBm (or 31.6 μW) in the ISM 868-MHz frequency band and for a 10-kΩ resistive load. This is based on a microstrip coupled transmission line allowing differential feeding, and on the use of two SMS7630 surface-mount Schottky diodes (on the SMS7630-005LF implementation) from Skyworks (Irvine, CA, USA) [54], which are mounted in doubler configuration. A shunt surface mount capacitor is used at its output as a

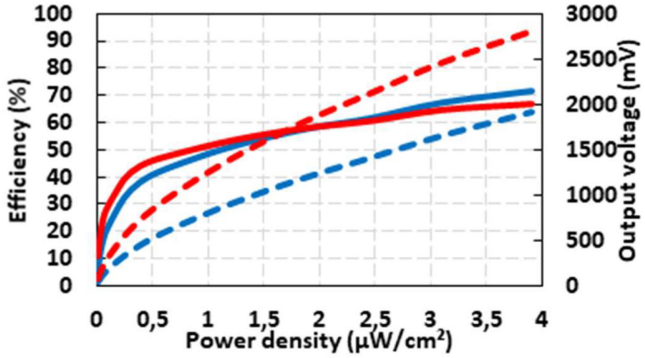

Fig. 9. Computed efficiency (full lines) and measured output dc voltage (dashed lines) against power densities for the printed folded quart-wavelength dipole rectenna with capacitive arms without (blue) and with (red) the use of a 6 cm × 8 cm reflector plane located at 5 cm below the antenna/rectenna, at 868 MHz and for a 10-kΩ resistive load.

low-pass filter, while an "L"-topology impedance matching network is used at its input. This last circuit is used in order to ensure the maximal power transfer from the antenna to the diodes, and is composed of a surface-mount inductor and a surface mount capacitor, both lumped, in order to get a 50-Ω impedance at the input of the full rectifier. The rectifier has a reflection coefficient (S_{11}) of −19 dB at the input port, a nearly 330-mV output voltage, an almost 35% efficiency (defined as the ratio between the output power on the input power), that says an output power of nearly 11 μW for a −15 dBm (or 31.6 μW) input, and has a 60-MHz bandwidth.

A rectenna composed of the printed folded quart-wavelength dipole antenna with capacitive arms (presented in Fig. 6) and of the full-wave rectifier designed for FR4 substrate (presented in Fig. 8) was designed and tested. Its efficiency (η_{rectenna}) (3) for a 10-kΩ resistive load at 868 MHz, represented in Fig. 9, is computed thanks to the measured output dc power of the rectifier (P_{dc}) and the estimated input radiative electromagnetic (or radio frequency) power of the antenna (P_{RF}) (4). This can also be expressed as the product of the incident electromagnetic power density (S) (5) by the effective area of the antenna (A_{eff}) (7). The incident electromagnetic power density (S) (5) can be estimated thanks to the effective electric field (E) (6) and the power generated by the radiative electromagnetic source (P_{TX}), the gain of the antenna used by the radiative electromagnetic source (G_{TX}), and the distance between the radiative electromagnetic source and the rectenna (d). The effective area of the antenna (A_{eff}) (7) can be estimated thanks to the gain of the antenna used by the rectenna (G_{RX}) and the wavelength (λ)

$$\eta_{\text{rectenna}} = \frac{P_{\text{DC}}}{P_{\text{RF}}} = \frac{P_{\text{DC}}}{S \cdot A_{\text{eff}}} = \frac{16 \cdot \pi^2 \cdot d^2}{P_{\text{TX}} \cdot G_{\text{TX}} \cdot G_{\text{RX}} \cdot \lambda^2} \cdot P_{\text{DC}} \quad (3)$$

$$P_{\text{RF}} = S \cdot A_{\text{eff}} = \frac{P_{\text{TX}} \cdot G_{\text{TX}} \cdot G_{\text{RX}} \cdot \lambda^2}{4 \cdot \pi \cdot d^2 \cdot 4 \cdot \pi} = \frac{P_{\text{TX}} \cdot G_{\text{TX}} \cdot G_{\text{RX}} \cdot \lambda^2}{16 \cdot \pi^2 \cdot d^2} \ (W) \quad (4)$$

$$S = \frac{E^2}{120 \cdot \pi} = \frac{30 \cdot P_{\text{TX}} \cdot G_{\text{TX}}}{120 \cdot \pi \cdot d^2}$$

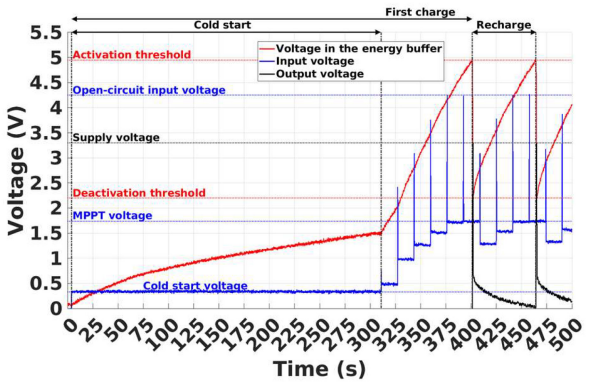

Fig. 10. Voltages, during a cold-start, a complete first charge and then a recharge, at the input of the Texas Instruments BQ25504 PMU (blue), in the energy buffer (red), and at the output of the Texas Instruments TPS63031 dc-to-dc buck-boost converter (black), for an input power of +0 dBm at 868 MHz.

$$= \frac{P_{TX} \cdot G_{TX}}{4 \cdot \pi \cdot d^2} \left(W \cdot m^{-2} \right) \tag{5}$$

$$E = \frac{\sqrt{30 \cdot P_{TX} \cdot G_{TX}}}{d} \left(V \cdot m^{-1} \right) \tag{6}$$

$$A_{eff} = G_{RX} \cdot \frac{\lambda^2}{4 \cdot \pi} \left(m^2 \right). \tag{7}$$

Several improvements can be achieved in order to increase the efficiency of the rectenna, concerning both the antenna and the rectifier, but also the connection between these.

e) Power management unit: To implement the "store then use" strategy, a PMU must be employed. This must efficiently scavenge the dc electrical power provided by the rectifier, efficiently store it in the energy buffer, and efficiently use the stored energy, once enough is available, to power the data management subsystem. It must properly work with the lowest possible input power and the lowest possible start-up voltage, but also present the lowest possible quiescent currents and sufficient output voltage and current.

A BQ25504 PMU from Texas Instruments (Dallas, TX, USA) has been chosen [55]. This can be controlled through threshold voltages from the energy buffer, provide a hardware maximum power point tracking (MPPT) system to optimize the power transfer from the rectifier to the energy buffer, and is able to cold-start, therefore, to operate even with an empty energy buffer. In order to smooth out the current draw and to provide a 3.3-V constant voltage to the load when enough energy is available, as presented in Fig. 4, a TPS63031 dc-to-dc buck-boost converter from Texas Instruments (Dallas, TX, USA) is used [56].

As presented in Fig. 10, if the energy buffer is empty, the PMU will use its cold-start ability to start storing the available input power in this last. When a sufficient voltage is reached, the hardware Maximal Power Point Tracking system is powered-up and will allow to optimize the power transfer from the input to the energy buffer. In fact, this circuit will sample the open-circuit input voltage every 16 s to impose on the input a ratio of it. This ratio is configurable with a resistor divider, and is currently set to 40% of the open-circuit input voltage. Then, when the voltage in the energy buffer reaches the activation threshold, the power good indicator will be raised and will activate the power supply of the data management subsystem. The energy buffer will start its discharge. When the voltage in the energy buffer will reach the deactivation threshold, the power good indicator will be turned down and will deactivate the power supply of the data management subsystem. Thus, the activation and deactivation thresholds, configurable with resistor dividers, allow to control the charge and discharge levels of the energy buffer. And this process will be periodically done as long as sufficient power is available at the input. It must be noted that undervoltage (to prevent the deep discharge), overvoltage (to prevent the over charge) and overheating protection mechanisms are available and configurable with resistors.

To work properly, this PMU requires a typically 15-μW input power during the cold-start and at least 10 μW during the normal charging, and this dc-to-dc buck/boost converter has maximum losses of 4.725 μW (disable and with an input power of 5.25 V) and 1.62 μW at the end of the cold-start (with a voltage of 1.8 V). Thus, at least around 14.725 μW are needed by these components to work properly during the normal charging, and 16.62 μW during the cold-start. Some other PMUs requires less energy. This is the case for the BQ25505 [57] and BQ25570 [58] from Texas Instruments (Dallas, TX, USA), which present the same behavior and similar performances, and which require a typically 15-μW input power during the cold-start and at least 5 μW during the normal charging. As well, the AEM30940 from e-peas (Mont-Saint-Guibert, Belgium) requires a typically 3-μW input power during the cold-start and at least -19 dBm (or 12.5 μW) during the normal charging [58].

By properly designing the combination between the capacitance (C) of the energy buffer and the activation (V_{act}) and deactivation (V_{deac}) thresholds voltage of the PMU, it is possible to ensure that enough energy (E) is stored to correctly power the data management subsystem

$$E = \frac{C}{2} \cdot \left({V_{act}}^2 - {V_{deact}}^2 \right). \tag{8}$$

f) Energy buffer: Conjointly designed with the PMU, the energy buffer must be able to store enough energy to power supply the data management subsystem for an entire process, as presented in Fig. 4. Also, the SNs must work for several decades and require some milli-joules to a few tens of milli-joules of energy to properly work. The required amount of energy is a function of the components (sensor, MCU, transceiver) and of their configuration (for the wireless communication: frequency band, output power, data rate, etc.). Thus, to provide a battery-free solution, the choice fell on the supercapacitors (or eventually capacitors or bank of capacitors). Indeed, the batteries have a limited lifetime, must eventually be recharged, but also have too large capacitances, while supercapacitors (and capacitors or bank of capacitors) have a wide range of low to medium capacitances and theoretical very long lifetime (expressed in millions of cycles). In fact, the choice is made according to the targeted capacitance (related to the maximum activation and minimum deactivation threshold voltages of the PMU) and in order to minimize the

self-discharge currents and losses. Regarding the technology, the supercapacitors that store the energy in an electrostatic way [e.g., electric double layer capacitors (EDLC)] have been favored, if available, over those that store the energy in an electro-chemical way (e.g., polarized aluminum electrolytic supercapacitors). This allows having a better ratio between energy and power densities, a longer lifetime, a lower self-discharge current and a lower sensitivity to the environment.

For the implementation of SNs, two different supercapacitors have been employed related to the energy required and by adding a margin to compensate the variability between components and the alterations over time: a 22-mF electric double layer capacitor from AVX Corporation BestCap (Greenville, SC, USA) [60] for storing up to 250 mJ, and a 2.2-mF polarized aluminum electrolytic supercapacitor from Panasonic (Kadoma, Osaka, Japan) [61] for storing up to 21 mJ. These have been chosen according to their capacitance and because providing the lowest self-discharge currents among the available solutions at the date of manufacturing. So, in the worst cases, the 22-mF supercapacitor requires 26 μW to compensate its highest losses for the maximum activation threshold voltage and 9 μW at the end of the cold-start, while, respectively, 606 and 71 μW for the 2.2-mF supercapacitor. Supercapacitors with higher capacitances could be used, but regarding the energy stored and unavailable (all the one under the deactivation threshold voltage), this is not relevant and even less energy efficient. Moreover, to be more energy efficient, the deactivation and activation threshold voltages must be minimized in order to limit the energy uselessly stored and to limit the maximum leakage current which is a function of the voltage.

g) Theoretical estimation of the range of use: Currently, this is the WPT which is limiting in terms of range of use and not the wireless communications. This limitation is imposed by the minimum input power required by the power management subsystem and its global efficiency. By considering the minimum power required by the power management subsystem to properly work (function of the rectenna efficiency, of the power required by the PMU, and of the power lost by the energy buffer), it is possible to estimate the maximum range of use in the worst case and for direct line of sight condition. This estimation is based on (3).

Thus, in the worst cases and with the 2.2-mF supercapacitor, a minimum input power of 87.62 μW is required to be almost certain to obtain a proper work of the power management subsystem during the cold-start, and at least 620.725 μW during the normal charging. With the 22-mF supercapacitor, these powers are, respectively, 25.62 and 40.725 μW. By using a model of the rectenna efficiency against power densities, based on the measured results presented in Fig. 9, and approximated by a logarithmic function for the lowest power densities (best correlation), it has been possible to estimate the minimum power density required in the worst use case for the normal charging and the cold-start, with the +1.540-dBi gain of the printed folded quart-wavelength dipole rectenna with capacitive arms, and for a +33 dBm (or +3 dB, or 2 W) radiative electromagnetic power source at 868 MHz. From this value, the estimation of the maximum range of use of the WPT system in this fixed configuration has been computed.

Thus, for the 2.2-mF supercapacitor, a power density of 1.205 μW·cm^{-2} (i.e., −7.87 dBm or 163.3 μW harvested) for the cold-start and of 6.524 μW·cm^{-2} (i.e., −0.54 dBm or 884.2 μW harvested) for the normal charging are required. This corresponds to a maximum range of use of the WPT system of, respectively, 3.63 and 1.56 m. By using a metallic reflector plane, which increases the gain up to +5.00 dBi, these ranges are increase up to 4.94 and 2.21 m.

Thus, for the 22-mF supercapacitor, a power density of 0.462 μW·cm^{-2} (i.e., −12.04 dBm or 62.6 μW harvested) for the cold-start and of 0.667 μW·cm^{-2} (i.e., −10.45 dBm or 90.2 μW harvested) for the normal charging are required. This corresponds for a maximum range of use of the WPT system of, respectively, 5.86 and 4.88 m. By using a metallic reflector plane, which increases the gain up to +5.00 dBi, these ranges are increase up to 8.34 and 6.93 m.

Nevertheless, these results are obviously only very simplified theoretical estimations in the worst case, considering only the unique path through the direct line of sight (no multipath propagation, nor interferences), and for a 10-kΩ resistive load. In the case of the targeted load (the power management subsystem), because of a variation of its input impedance and more generally of its properties (function of the input and the outputs, such as the voltage in the energy buffer), it is not feasible to obtain in a simple way the efficiency against power densities measurement for the rectenna.

Several improvements in the design can be carried out in order to increase the range of use. First, more efficient components can be used: rectifier with higher efficiency, PMU requiring less power, and energy buffer with lower losses. Second, the energy required by the data management part can be reduced: in that way, the capacitance could be reduced and/or the activation threshold voltage could be decreased, this tends to reduce the maximum losses of the energy buffer. By reducing the required power in the worst case, it becomes possible to use the SNs with lower power densities and, thus, on wider ranges. Moreover, the lower the required energy, the faster the charging time, and for equivalent power losses, the lower the energy losses.

h) Strategy of control: The SNs are inaccessible once deployed. This inaccessibility is both hardware and software: there is no means to have a physical access (because buried into reinforced concrete) and no mean to have a wireless digital access (because designed without data downlink). Neither the hardware nor the software can be updated or replaced, and also, these must work for long term. Moreover, the periodicity of functioning is not controlled by the software (e.g., with events or timer interruptions). Even though there are no conventional way to control the SNs, their periodicity of functioning can be wirelessly and remotely controlled by the CNs through the power downlink achieved by the WPT. This control can be performed by tuning their wireless power source in terms of waveform, output power, and/or periodicity of activation/duty cycle.

To be efficient, this strategy of control must be based on the knowledge of the CNs of the energy needs of each SN

located in their neighborhood (in terms of the power required and of the duration of the power supply). For instance, by considering that a unique CN requires H hours to wirelessly power all the SNs in its neighborhood, and if a measurement is required each H hours, the CN can activate continuously its power source. However, if a measurement is required each D days, it can activate its power source only H hours each D days, or reduce the transmission power and adapt the duration (higher than H hours) at the condition that all the SNs can always harvest enough power.

It should be noted that because of the "store then use" strategy, the periodicity of activation of each SN in the neighborhood of a same CN is a function of the available electromagnetic power and, thus, it is specific for each SNs. Also, this periodicity is a function of: the distance between the SN and the CN; the relative orientation and polarization matching between the antennas of the SN and CN; the electromagnetic properties of the propagation medium (e.g., metallic rebars position, humidity rate); etc. The temporal characterization of the SNs allows to estimate the time required for the CN to power or interrogate all the SN accessible in its neighborhood. The same SN will transmit several measured data during a specific time slot and, thus, it allows the temporal redundancy. As a large majority of SNs are accessible during a measurement campaign, a good spatial precision can be obtained. If some SNs are nonreachable, the spatial redundancy allows to have enough precision. Finally, the variability in periodicity of activation of the SNs is an efficient way to avoid collisions and interferences during data transmissions, which is already limited by the design of the LoRaWAN technology.

To go further, we could consider the case of several fleets of SNs, where each fleet is dedicated to the measurement of specific parameters and whose frequency band dedicated to the WPT does not overlap the bands of the other fleets. Thus, each fleet can be discriminated by the configuration of their WPT interface, and can be powered independently. In consequence, by tuning both the central frequency and the bandwidth of the generated radiative electromagnetic power by the CNs, it becomes possible to power only a part of the fleets of SNs, or to provide at each one a different periodicity of functioning.

To increase the end-to-end efficiency, beamforming [62], [63], [64] and/or frequency diverse arrays (FDAs) [65], [66] solutions can be applied in the radiative electromagnetic power source to independently or/and individually power each SN.

i) Implementation of the sensing nodes: Several prototypes of SNs have been manufactured, as presented in Fig. 11 [16]. These use a unique antenna with a radio-frequency circulator, have a printed circuit board (PCB) embedding the data management and the power management subsystems, and present some interface to connect the different kinds of sensors available on daughter boards. The implemented firmware specifies the unique identifiers, and is a function of the chosen sensor and of the chosen configuration for the wireless communication.

III. Experimental Results

Several SNs have been implemented, tested and characterized [16], [17], [18], in particular four in the latest version which are those presented in this section. Their power consumption versus the configuration of the wireless communication and versus the used sensor, the duration of the first charge and of recharges, the required minimum radiative electromagnetic power as well as the estimated maximum range of use, the reproducibility (study based on all the SNs implemented regardless their version), the efficiency, and the test in various configurations are key elements to certify the good functioning of the proposed SNs.

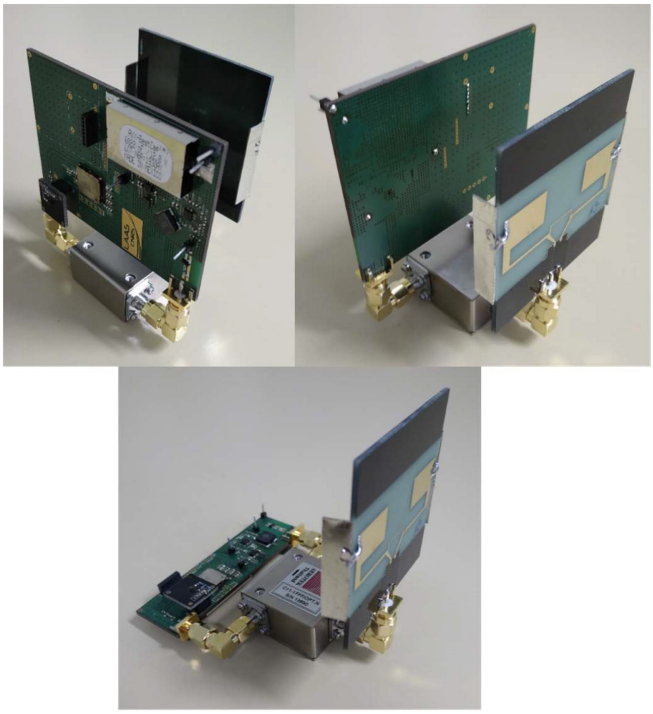

Fig. 11. Photographs of prototypes of the SNs, using or not the PCB as a 6 cm × 8 cm metallic reflector plane located at 5 cm below the unique antenna.

A. Characterization of the Power Consumption

The power consumption of the data management subsystem constraints the design of the power management subsystem. This power consumption depends on the configuration of the wireless communication (in particular the transmission power, the data rate (related to the duration of the transmission), and the size of the data payload); and on the sensor used. The objective is to provide the best tradeoff between the reliability of the wireless communication and the power consumption. Furthermore, both hardware and software optimizations can still be performed to minimize as much as possible the energy required.

Currently, the LoRaWAN wireless communication technology is employed. Each communication slot is composed of a 17-bytes long LoRaWAN frame, whose 13 bytes are dedicated to the LoRaWAN protocol and 4 bytes dedicated to the data payload. Whatever the sensor used, the data payload could be reduced regarding the quantity of data to send (currently two) and by optimizing the data format (currently each data is formatted on two bytes). By reducing the data payload, it is possible to shorten the wireless transmission and to reduce

the energy required for it. Generally, the energy required for the wireless transmission is higher than the energy required for the other processes (initialization, measurement, data formatting, etc.). For all the tested SNs, the energy required for their initialization is quite similar (11.3 mJ in average), whatever the configuration of the wireless communication and the sensor used.

1) Power Consumption Versus Transmission Power: The transmission power is the first parameter of the configuration of the wireless communication which can be optimized. Indeed, the higher the transmission power is, the higher the energy required. Nevertheless, the lower the transmission power is, the shorter the range.

Fig. 12 presents the power consumption of the SNs versus the transmission power, for a fixed data rate of 250 bps (DR0) and 4 bytes of data payload. For this data rate and this data payload, the data transmission lasts 1318.9 ms. The used LoRa module allows transmission power between +4 and +16 dBm, with a step of +2 dBm. Thus, 160.5 mJ in average (or 40.125 mJ per data byte, or 9.44 mJ per transmitted byte, or 1.18 mJ per transmitted bit) are required for a +14-dBm wireless transmission and 80.6 mJ (or 20.15 mJ per data byte, or 4.74 mJ per transmitted byte, or 0.59 mJ per transmitted bit) in average for a +4-dBm wireless transmission. Therefore, by reducing the transmission power from +14 to +4 dBm, the energy required for the wireless communication is almost halved, and the range of use is always sufficient: at least tens of meters even from a reinforced concrete beam and indoors.

2) Power Consumption Versus Data Rate: The data rate is another parameter of the configuration of the wireless communication which can be optimized. Indeed, the faster the data rate is, the shorter the duration of the data transmission, and the lower the energy required. Nevertheless, the faster the data rate, the shorter the range is (because the demodulation becomes more complex).

Fig. 13 presents the power consumption of the SNs versus the data rate, for a fixed power transmission of +4 dBm and for a 17-bytes long LoRaWAN frame. For 4 bytes of data payload, the data transmission lasts 1318.9 ms with the data rate of 250 bps (DR0) and 51.5 ms with the data rate of 5470 bps (DR5). Thus, 80.6 mJ (or 20.15 mJ per data byte, or 4.74 mJ per transmitted byte, or 0.59 mJ per transmitted bit) in average are required for a wireless transmission at a data rate of 250 bps, and 4.68 mJ in average (or 1.17 mJ per data byte, or 0.28 mJ per transmitted byte, or 34 μJ per transmitted bit) for a wireless transmission at a data rate of 5470 bps. Thus, by increasing the data rate from 250 to 5470 bps, the energy required for the wireless communication is almost divided by 17, and the range of use is always sufficient: at least a few tens of meters even from a reinforced concrete beam and indoors. For the fastest data rate, the energy required for the wireless transmission is lower than the energy required for the other processes (initialization, measurement, data formatting, etc.). In this case, further optimizations—especially in the low-level software—must be achieved to reduce the overall power consumption of the SNs.

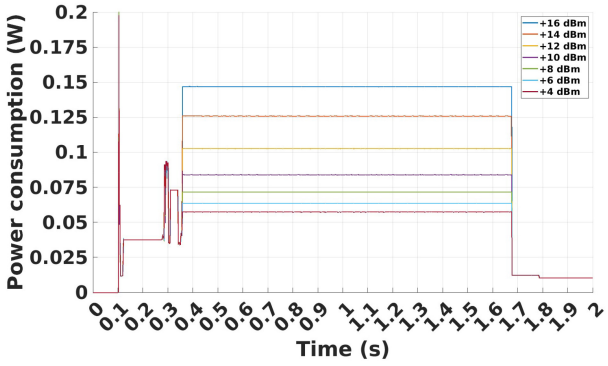

Fig. 12. Power consumption of the SN against the data transmission power, for the slowest data rate (DR0) and a 4-bytes data payload.

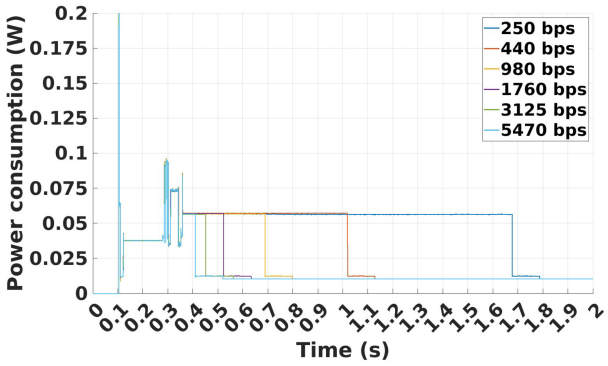

Fig. 13. Power consumption of the SN against the data rate, for a +4-dBm transmission power and a 4-bytes data payload.

3) Power Consumption Versus Sensor: Because the SNs are designed in order to be generic platforms where different kinds of sensor can be connected *via* specific daughter boards, the power consumption of each sensor must be limited. Consequently, these must be low power, have similar energy requirements and provide a similar amount of data in order to transmit a LoRaWAN data frame of similar length and duration.

Fig. 14 presents the power consumption of the SNs all based on an identical version of the electronic board versus the sensor connected on the board with a specific daughter board and with the associated firmware. The measurements are for a fixed power transmission of +4 dBm, a fixed data rate of 5470 bps and for a 17-bytes long LoRaWAN frame with 4 bytes of data payload. Thus, the HDC2080 sensor from Texas Instruments (Dallas, TX, USA) requires 0.56 mJ of additional energy, the thermodiodes 3.03 mJ, the strain gauge 4.81 mJ, and the resistivity sensor 3.16 mJ. These additional energies are limited and can be minimized by hardware optimizations, especially on the daughter boards. By considering this diversity, the power management subsystem can be tuned to make the SNs generic in terms of the employed sensors. Also, the simultaneous use of multiple sensors must be investigated.

4) Overall Power Consumption: Finally, the energy required for a complete process depends on the configuration of the wireless communication (including transmission power and data rate), and is little influenced by the sensor used. Thus, for the transmission of 4 bytes of data payload in a

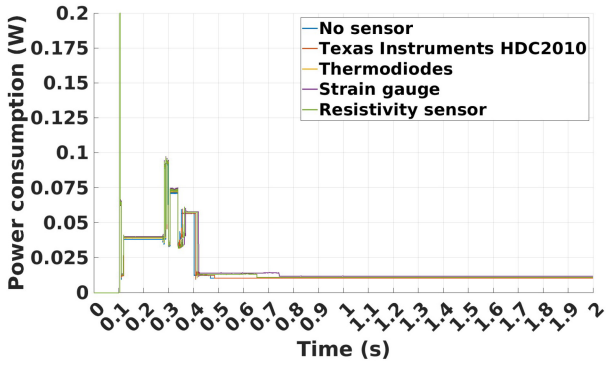

Fig. 14. Power consumption of the SN against the sensor, for the fastest data rate (DR5), a 4-bytes data payload, and a +4-dBm transmission power.

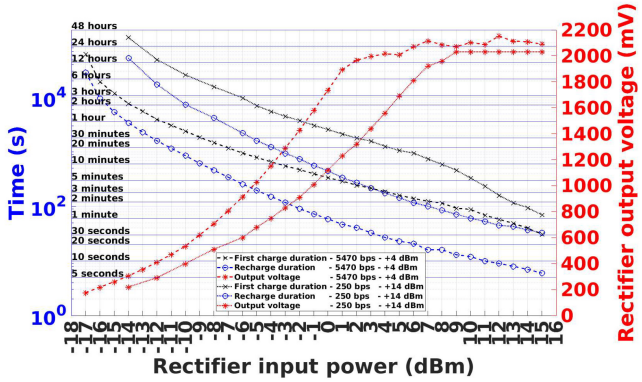

Fig. 15. Durations of the first charge ("x," left) and recharges ("o," left), and rectifier output voltages in open-circuit during the recharges ("*," right) against the conducted electromagnetic input power applied at the input of the rectifier of the SNs, for a frequency of 868 MHz, and for two configurations of the wireless communication: transmission power of +4 dBm and data rate of 5470 bps (dashed lines), and transmission power of +14 dBm and data rate of 250 bps (dotted lines).

17-bytes long LoRaWAN frame, in the worst case for the most reliable configuration of the wireless communication (transmission power of +14 dBm, and data rate of 250 bps) 210 mJ are required. On the other hand, in the worst case for the less reliable configuration of the wireless communication (transmission power of +4 dBm, and data rate of 5470 bps), that still meets the requirements, 20 mJ are required. By using the average energy required and by adding 20% to compensate the variability and the aging, 250 mJ are stored in the first case and 21 mJ in the second. This represents, respectively, 62.5 mJ of stored energy per data byte (or 14.71 mJ of stored energy per transmitted byte, or 1.84 mJ of stored energy per transmitted bit); and, respectively, 5.25 mJ of stored energy per data byte (or 309 mJ of stored energy per transmitted byte, or 39 μJ of stored energy per transmitted bit).

B. Temporal Characterization of the Duration of the First Charge and Recharges Versus the Available Input Power

The duration of the first charge and recharge gives a good approximation of the shortest periodicity of functioning of the SNs possible depending on the available power it can harvest and, thus, indirectly of the distance to the power source(s). The energy to be stored by the power management subsystem and its efficiency constraint the duration of a first charge (from an empty energy buffer) and of recharges (from a previous complete charge). The efficiency is highly impacted by the efficiency of the rectenna, the power required by the PMU to work, and by the power losses of the dc-to-dc converter and of the energy buffer, the latter is the function of the applied voltage. The objective is to provide the most efficient power management subsystem with the fastest charges and the lowest possible required input power to ensure the widest possible ranges. Moreover, hardware optimizations can still be performed in order to improve as much as possible the efficiency.

1) Duration of the First Charge and Recharges Versus the Available Input Power: The characterization presented in Fig. 15 has been performed at 868 MHz, which is within a few MHz of the frequency to get the optimum use of the rectifier, and by applying a conducted electromagnetic power at the input of the radio-frequency circulator to transmit it to the input of the rectifier. The durations are computed by using the timestamps provided by the CN for each received LoRaWAN frame transmitted by the SN under test.

Most of the first charges are performed under the cold-start process, during which an input voltage of around 330 mV is imposed by the PMU, as presented in Fig. 10, which does not allow optimizing the power exchange between the rectenna and the energy buffer. Indeed, the rectifier is more efficient for higher voltages by considering the same input power. Once the cold-start is achieved, thanks to the activation of the hardware MPPT system, the power exchange between the rectenna and the energy buffer is improved. It must be noted that the rectifier output voltage saturates for the highest input powers. Generally, the lower the energy to be stored, the faster the charge; and the lower the available input power, the slower the charge.

For the less reliable configuration of the wireless communication (transmission power of +4 dBm, and data rate of 5470 bps) which requires 21 mJ to be stored, the SNs can work with an input down to −17 dBm (or 20.0 μW) provided by the antenna to the radio-frequency circulator and at least up to +15 dBm (or 31.6 mW). Thus, the first charge lasts from around 17 h and 21 min, to around 30 s, while the recharges from around 7 h and 59 min, to around 6 s.

For the most reliable configuration of the wireless communication (transmission power of +14 dBm, and data rate of 250 bps) which requires 250 mJ to be stored, the SNs can work with an input down to −14 dBm (or 39.8 μW) provided by the antenna to the radio-frequency circulator and at least up to +15 dBm (or 31.6 mW). Thus, the first charge lasts from around 34 h and 36 min, to around 1 min and 10 s, while the recharges from around 14 h and 38 min, to around 33 s.

Therefore, longer periodicities can be obtained by controlling the duration and periodicity of activation of the power source by the Communication Node(s) and, thus, without altering neither the software nor the hardware of the SNs.

2) Minimum Input Power and Experimental Estimation of the Range of Use: As a reminder, the estimation of the

maximum range to operate properly the SNs according to the theoretical minimum required input power in function of the employed supercapacitor and in the worst case, are, respectively, for the cold-start and the normal charging, for the 2.2-mF capacitance: 3.63 and 1.56 m with the +1.54-dBi gain antenna, and 4.94 and 2.21 m with the +5.00-dBi gain antenna; and for the 22-mF capacitance: 5.86 and 4.88 m with the +1.54-dBi gain antenna, and 8.34 and 6.93 m with the +5.00-dBi gain antenna. These worst cases have apparently never been met during the various tests and characterization carried out. Indeed, the SNs have properly operated for power at the input of the radio-frequency circulator down to −17 dBm (or 20.0 μW) and –14 dBm (or 39.8 μW), respectively, for the less and the most reliable configurations of the wireless communication, both for the cold-start and normal charging.

Thus, by applying the Friis equation, the distance between a CN and specifically its EIRP of +33 dBm (or +3 dB, or 2 W) in the 868-MHz ISM frequency band, and an SN equipped with the +1.54-dBi gain antenna can be estimated in the function of the required input power obtained experimentally. Thus, −14 dBm (or 39.8 μW) can be harvested at a distance of around 7.35 m and −17 dBm (or 20.0 μW) at around 10.38 m, and around −10.6 dBm (or 87.1 μW) can be harvested at a distance of 5 m. By using a metallic reflector plane to get the +5.00-dBi gain antenna, −14 dBm (or 39.8 μW) can be harvested at a distance of around 10.95 m and −17 dBm (or 20.0 μW) at around 13.78 m, and around −7.2 dBm (or 190.5 μW) can be harvested at a distance of 5 m.

It must be noted that a −17 dBm (or 20.0 μW) as the minimum power at the output of the antenna is one of the lowest found in the literature. The the best of our knowledge, only [59] provides a power management subsystem which needs −19 dBm (or 12.5 μW) in the 868-MHz ISM frequency band and −19.5 dBm (or 11.2 μW) in the 915-MHz ISM frequency band.

C. Study of the Reproducibility

In order to quantify the number of iterations to consider to be able to provide a relevant estimation of the average value from the measured data, few statistical analyses have been carried out.

1) Reproducibility for Sensing Node: First, the variability for each SN has been measured. Because of the very long time required for the measurements, the study has been limited to two conducted electromagnetic powers at the input of the radio-frequency circulator: +15 dBm (or 31.6 mW) and +0 dBm (or 1.0 mW). Several sets of data have been produced at different times and under different environmental conditions, for SNs using a 22-mF supercapacitor. The sets dedicated to the first charges are also limited because of the required time of measurements.

Regarding the duration of the recharges for a power of +15 dBm (or 31.6 mW), the average is closely similar in the various sets and the standard deviation is limited around 3.94% (or 1 s, that says the measurement step). Hence, the deviations

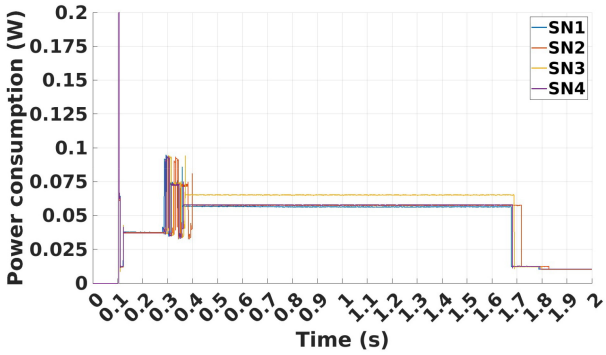

Fig. 16. Power consumption of the SNs for a transmission power of +14 dBm and the slowest data rate (DR0).

can be mainly explained by the measurement precision (1 s) and by the functioning of the hardware MPPT system. Indeed, this achieves a sampling of the input open-circuit voltage each 16 s for nearly 256 ms, and matches its input impedance in the function of the sampled voltage and the voltage in the energy buffer. Depending on the time in the charge when the sampling takes place, (e.g., just after the discharge, just before the discharge, etc.), the impedance matching will be different, and the voltage provided by the rectifier will vary, all that will induce nonnegligible time variation for the short recharges.

Regarding the duration of the first charge for a power of +15 dBm (or 31.6 mW), the average is closely similar in the various sets and the standard deviation is limited to 1 s (or 0.88%), that says the measurement step. Thus, the deviations can be mainly explained by the measurement precision (1 s).

Regarding the duration of the recharges for a power of +0 dBm (or 1.0 mW), the average is closely similar in the various sets and the standard deviation is limited to few seconds, that says around 1.15%.

Regarding the duration of the first charge for a power of +0 dBm (or 1.0 mW), the average is closely similar in the various sets and the standard deviation is around 2.56%.

From these observations, it has been decided to consider the average value for at least ten measurements in order to conserve a relevant order of magnitude.

2) Reproducibility Between Sensing Nodes: As presented in Figs. 16 and 17, there are few variations between the power consumption of different SNs. These differences are mainly due to the variability in the components. In consequence, this variability is around 4.2% and is compensated in the design of the SNs by the 20% overestimation in the quantity of energy to store.

D. Study of the Efficiency

One of the figures of merit of the SN is the energy efficiency. This is defined here as the ratio of the energy available at the input of the SN (i.e., the power available at the input of the SN (the one harvested by the antenna) integrated over the period of interest) to the energy required for a complete process. This criterium must be considered in order to provide a sustainable system.

According to Fig. 18, the efficiency is rather low for the first charge: between 2.16% and 11.54% for the SN with the

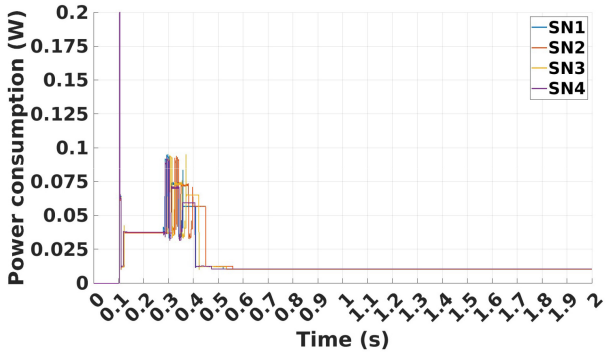

Fig. 17. Power consumption of the SNs for a transmission power of +4 dBm and the fastest data rate (DR5).

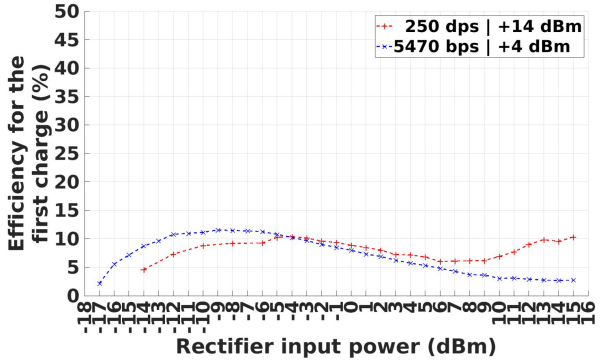

Fig. 18. Energy efficiency of the SNs during the first charge against the conducted electromagnetic input power applied at the input of the rectifier, for a frequency of 868 MHz, and for two configurations of the wireless communication: transmission power of +4 dBm and data rate of 5470 bps (blue), and transmission power of +14 dBm and data rate of 250 bps (red).

less reliable configuration of the wireless communication and a 2.2-mF supercapacitor; and between 4.59% and 10.25% for the SN with the most reliable configuration of the wireless communication and a 22-mF supercapacitor; and according to Fig. 19, the efficiency is increased for the recharges, respectively: between 3.68% and 36.71%; and between 7.91% and 39.00%. It must be noted that the two configurations do not present their peak of efficiency for the same input power. These are, respectively, reached at −9 dBm and at −5 dBm for the first charge, and at −2 dBm and at +1 dBm for the recharges. In addition, the first configuration is more efficient for the lowest input powers, and the second for the highest.

To improve the efficiency of the SN, the duration of the first charge and recharges must be minimized.

Another efficiency which could be relevant to express is the one defined as the ratio of the energy transmitted by a CN to wirelessly power all the SNs located in its neighborhood, to the sum of the energies consumed by each SN during a period of interest. In this case, the more SNs there are, the higher the overall efficiency; and the higher the efficiency of each SN, the higher the overall efficiency.

E. Qualitative Results

To certify the proper functioning of the complete CPS, and of each of its components (namely, the SNs and the CNs)

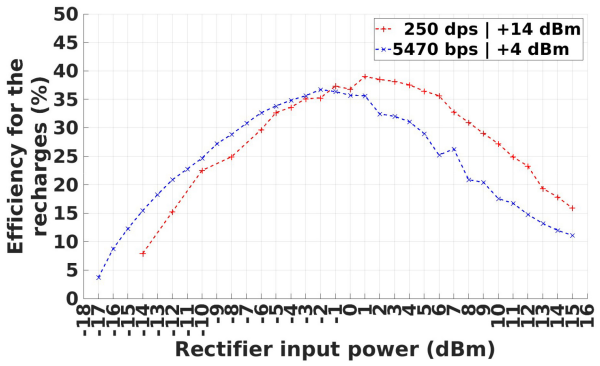

Fig. 19. Energy efficiency of the SNs during the recharge against the conducted electromagnetic input power applied at the input of the rectifier, for a frequency of 868 MHz, and for two configurations of the wireless communication: transmission power of +4 dBm and data rate of 5470 bps (blue), and transmission power of +14 dBm and data rate of 250 bps (red).

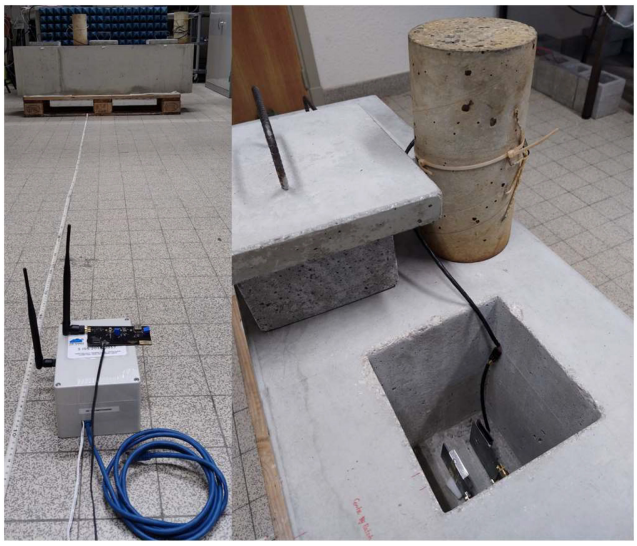

Fig. 20. Photographs of a complete CPS composed of three SNs embedded in a reinforced concrete beam, and of one CN.

several qualitative tests have been successfully performed, in several configurations.

For instance, a CPS composed of a meshed network of two CNs (only 1 with a connection to the Internet) and four SNs, whose tree located in the air cavities of a reinforced concrete beam, as partially presented in Fig. 20, have successfully been deployed and tested for temperature, relative humidity and electrical resistivity measurements. In this setup, a CN has wirelessly powered and controlled over meters (at least 3 m, with at least 15 cm of reinforced concrete) the SNs embedded in the reinforced concrete beam or located close to. It was observed that the two CNs received all the data sent by the SNs over at least a few tens of meters, and processed, stored and shared these in the meshed Network and with the digital world *via* the Internet. Obviously, a unique CN can easily manage several SNs omnidirectionally over several meters.

Moreover, indoors tests have allowed to successfully power and control SNs with a unique CN at a distance of 11 m in the air, and it seems possible to achieve wider ranges.

Other relevant tests concern the use of the wireless power source in the air cavities of the reinforced concrete beam. With the power source in the central air cavity, it has been possible to power SNs located in the two other air cavities, that says, through at least 30 cm of reinforced concrete, but also other SNs located outside the reinforced concrete beam and over some meters. Finally, by locating the power source in one of the extremum air cavities and by filling the central air cavity with a reinforced concrete cap, an SN placed in the other extremum air cavity has been successfully powered, that says through at least 75 cm of reinforced concrete, in the case of a direct line of sight and without external reflection on the floor or wall.

During all the experiments, no LoRaWAN frame transmitted by the SNs (with a single or two different antennas) were lost. It should be noticed that the two antennas of the CNs (a transmitting antenna for the WPT, and a receiving antenna for the LoRaWAN data transfer) are located in the same reduced space and operate with the same linear polarization.

In conclusion, the qualitative tests have shown a strong disparity of the obtained results in function of the relative position of the SNs with respect to the reinforced concrete and to the CN(s). They have also shown a very wide disparity in the properties of the reinforced concrete, which highly affects the WPT [19].

IV. Discussion

The objective of this work is to design and implement a CPS based on the use of generic, low-power, fully wireless, fully buried, battery-free, and omnidirectionally, wirelessly and remotely over meters powered and controlled SNs, and which is dedicated to the SHM of reinforced concrete in its full life, i.e., for decades.

A. Current Solutions for the Structural Health Monitoring of Reinforced Concrete

Among the Smart Concretes as defined in the civil engineering industry [67], [68], [69], a major part targets the same objectives as the McBIM project, i.e., for the SHM: this is the self-sensing concretes. These can be intrinsic [68], [69], [70], [71] or nonintrinsic (or instrumented by embedding transducers and/or sensors) [68], [72], [73], [74], [75], [76] self-sensing, but can even be defined as "connected" [77], [78], [79], [80].

The current intrinsic [68], [69], [70], [71] and nonintrinsic [68], [72], [73], [74], [75], [76] self-sensing concretes are subjects of laboratory studies, which are not yet able to collect, store or transmit data without the use of an external equipment, generally connected by wires, complex, power consuming, and driven by an operator. Moreover, some of these are based on indirect measurements requiring signal processing, while others could be investigated to become transducers for SNs.

There are also wireless passive solutions which can be used for traceability or monitoring purposes, and which are based on radio-frequency identification (RFID) tags [81], [82], [83], [84], [85], [86], [87], [88] or on passive resonators [89], [90], buried into concrete. These are not yet able to collect, and then transmit data without the use of a wireless external "reader" usually driven by an operator who must know their location because of the short range of the employed wireless communication technologies based on backscattering. Furthermore, no or only very few amounts of data can be stored.

The other Smart Concretes are the instrumented ones, which are based on WSNs usually embedded on the surface or buried at a small depth in the concrete (with a maximum depth of 15 cm found in the literature), some are from academics [91], [92], [93], [94], [95], [96], [97], [98], [99], [100], [101] and others from industrials [102], [103], [104], [105], [106], [107], [108], [109], [110], [111], [112]. Table II summarizes the properties of the available SNs. Most of them use a wireless datalogger or a wireless transmitter manually placed on the surface, and which use one or several wired and sacrificed sensors buried in the concrete or placed on its surface. These solutions are increasingly using a wide variety of wireless communication technologies in order to remotely and digitally store and process the collected data. By removing the wires, the networks become more easily scalable, need less deployment time and, thus, are less expensive. Regarding the wireless communication, the useful range is between some meters and hundreds of meters. A battery powers all these solutions, and therefore, those of the accessible solutions must periodically recharge or change it, and for the inaccessible solutions their lifetime is limited to a few months or a few years. Among the commercially available solutions, only [112] provides ambient energy harvesting or WPT solution for powering the SNs.

All the current solutions can be deployed for low to medium term periods, often requiring external equipment, and can monitor, between others, the mechanical deformation, the moisture, the temperature, the pH, or the corrosion, but even detect and localize damages.

Moreover, the solutions based of WSNs allow to connect concrete [91], [92], [93], [94], [95], [96], [97], [98], [99], [100], [101], [102], [103], [104], [105], [106], [107], [108], [109], [110], [111], [112]. Another way to achieve this is to use embedded wireless tags (e.g., RFID, NFC, etc.) which provide some information such as an identifier or a uniform resource locator (URL) to wirelessly access through the Internet, the data in relation to the interrogate element [77], [78], [79], [80].

Nevertheless, few works deal with the recharge of the battery located in the concrete by the use of an inductive short-range WPT system [97], [98]. Also, few wireless sensors deployed on concrete elements are battery-free and wirelessly powered by a radiative WPT system [99], [101], [112]. Finally, few solutions of wireless sensors dedicated to the SHM of concrete structures use the ambient energy harvesting (from solar energy [113], [114] or mechanical vibrations [115]) to recharge batteries and extend their lifetime. However, none of these systems is designed to be buried into concrete to ensure its long-term SHM, and these are highly dependent on the environment of deployment, of the ambient energy sources and of the targeted application.

Regarding the evaluation of the corrosion, there are no current solutions which are based on low-power, battery-free, fully wireless, and fully buried SN [24]. Indeed, the

TABLE II
COMPARISON OF CURRENT SNS FOR THE SHM OF REINFORCED CONCRETE

Ref.	Manufacturer or publication date	Wireless communication technology (frequency)	Deployment strategy (impacting on ease of implementation)	Available sensor(s)	Power source	Estimated lifetime
[77]	Doka	Cellular (2G, 3G, 4G); BLE (2.45 GHz)	Node on concrete surface and sacrificed sensor in concrete	Temperature*	Battery	3 months
[78]	Concrefy	LoRa (868 MHz)	Node on concrete surface	Temperature*; pressure	Battery	N/A
[79]	360 SmartConnect	NFC (13.56 MHz)	Tag a few centimetres in concrete	N/A	Backscattering	Very long
[80]	idencia	RFID (13.56 MHz)	Tag on concrete surface	N/A	Backscattering	Very long
[102]	CAPTAE	Cellular (3G, 4G); RFID (13.56 MHz)	Node on concrete surface	Temperature*; humidity; strength/constraints; elastic and inelastic deformations; inclination; pressure; displacement; defects and shock detection; weather parameters; almost any type of sensor on request	Battery	Between 1 and 3 years
[103]	TELEMAC	Cellular (3G)	Wireless datalogger on concrete surface with 5 wired sacrificed sensors in concrete	Temperature*; humidity; strength/constraints; elastic and inelastic deformations; inclination; load/pressure; displacement; defects and shock detection	Battery	Between 5 and 10 years
[104, 118]	CEMENTYS	LoRa (868 MHz)	Wireless datalogger on concrete surface with 8 wired sacrificed sensors in concrete	Temperature*; humidity; strength/constraints; elastic and inelastic deformations; inclination; load/pressure; resistivity for corrosion estimation	Battery	N/A
[105]	itmsol	Cellular (2G, 3G); BLE (2.45GHz); LoRaWAN (868 MHz); SigFox (868 MHz); NB-IoT; LTE-M; other solutions on request	Wireless datalogger on concrete surface with up to 5 wired sacrificed sensors in concrete	Temperature*; humidity; strength/constraints; elastic and inelastic deformations; inclination; load/pressure; defects and shock detection	Battery	Between 7 months to 6.4 years
[106]	WAKE	Cellular; RFID (13.56 MHz); BLE (2.45 GHz)	Wireless datalogger on concrete surface with up to 24 wired sacrificed sensors in concrete	Temperature*	Battery	Between 4 months and 3 years
[107]	GIATEC	Cellular; Wi-Fi (2.45 GHz); BLE (2.45 GHz)	Node in concrete	Temperature*; strength/constraints	Battery	Up to 4 months
[108]	LumiCON	Cellular	Node in concrete	Temperature*; strength/constraints	Battery	N/A
[109]	HILTI	BLE (2.45 GHz); undefined LPWAN	Node in concrete	Temperature*; strength/constraints	Battery	2 months
[110, 111]	Maturix (Sensohive)	NFC (13.56 MHz); RFID (13.56 MHz); SigFox (868 MHz)	Node on concrete surface and sacrificed sensor in concrete	Temperature*; humidity; strength/constraints	Battery	N/A
[112]	GreenWake Technologies	Non-standardised (868 MHz)	Node on concrete surface	Temperature*; humidity; pressure; acceleration/inclination; magnetic field; luminosity; mechanical deformation	Radiative WPT (2.45 GHz) for battery-free node	Very long
[93]	2009	Non-standardised (2.45 GHz)	Node on concrete surface	Temperature*; humidity; deformations; luminosity; acceleration	Battery	Months
[101]	2009	ZigBee (2.45 GHz)	Node on concrete surface	Impedance	Radiative WPT (2.45 GHz) for battery-free node	Very long
[92]	2011	Non-standardised (433 MHz)	Node in concrete	Temperature*; humidity; impedance	Battery	N/A
[94]	2012	ZigBee (868 MHz)	Node in concrete	Temperature; humidity; electromechanical impedance	Battery	Nearly one month
[115]	2016	LoRa (868 MHz)	Node on concrete surface	Temperature*; humidity; car traffic (indirectly)	Mechanical energy harvesting (vibrations) for battery-free node	Long
[97, 98]	2017	Non-standardised (169 MHz)	Node in concrete	Temperature*; strength/constraints	Inductive WPT (100 kHz) to recharge battery	Months
[99]	2018	LoRaWAN (868 MHz)	Node on concrete surface	Temperature*	Radiative WPT (845 MHz) for battery-free node	Very long
[113]	2018	LoRaWAN (868 MHz)	Node on concrete surface	Crackmeter	Solar energy harvesting to recharge battery	10 years
[114]	2019	LoRaWAN (868 MHz)	Node on concrete surface	Temperature*; humidity; pressure; displacement; acceleration/inclination; magnetic field	Solar energy harvesting to recharge battery	N/A
[119]	2020	Wired (N/A)	Sensor in concrete and pseudo-node on concrete surface	Resistivity for corrosion estimation	External (laptop *via* USB)	N/A
This work	Since 2018	LoRaWAN (868 MHz)	Node in concrete	Temperature*; humidity; deformations; resistivity for corrosion estimation	Radiative WPT (868 MHz) for battery-free node	Very long

* Temperature measurements (that can be combined with humidity and/or strength measurements) are usually used during the curing phase in order to monitor the concrete maturity.
N.B.: Cost information for each Sensing Node is not available.

commercially available corrosion sensors for the reinforced concretes are usually placed on the surface of the reinforced concrete and have a limited life due to the use of batteries. These are based on the manual measurement of the surface electrical resistivity [116], [117]; or are buried in the near surface and are automatically driven by a datalogger [118]. Another solution is based on a passive sensor which can be locally interrogated by a magnetic field [89]. Finally, an electrical resistivity sensor fully buried in reinforced concrete is presented in [119], but this one is not yet able to wirelessly transmit the collected data, and is not energy autonomous. Consequently, to the best of our knowledge, the first generic SN dedicated to the SHM of reinforced concrete, which is fully buried, fully wireless, low-power, battery-free, wirelessly

TABLE III
COMPARISON OF CURRENT SOLUTIONS FOR THE WPT OF WSNS DEDICATED TO SHM APPLICATIONS

Reference	[101]	[112]	[122]	[126]	[123]	[124]	[125]	Previous version of this work [18]	This work
Date of publication	2009	2021	2017	2019	2021	2017	2018	Since 2018	
Wireless communication technology (frequency)	ZigBee (2.45 GHz)	N/A (N/A)	Bluetooth Low Energy (2.45 GHz)		LoRa (2.45 GHz)	DASH7 (433 MHz)	Bluetooth Low Energy (2.45 GHz)	LoRaWAN (868 MHz)	
Sensor	Impedance	Temperature*; relative humidity; pressure; acceleration; inclination; magnetic field; luminosity; mechanical deformation	Temperature* and relative humidity; acceleration		Acceleration	Temperature* and relative humidity	Temperature*; pressure; acceleration	Temperature* and relative humidity; dielectric resistivity; mechanical deformation	
Wireless Power Transfer frequency	2.45 GHz	2.45 GHz	868 MHz		2.45 GHz	868 MHz	868 MHz	868 MHz	
Transmitted power (dBm)	+30	+27 to +36	+23 to +35	+34.6	+27 (*2)	+27 or +33	+27	+33	
Range of input power (dBm)	N/A	-9 to +15	-10 to +5		N/A	From -17	From -10.5	-14 to +15	-17 to +15
Maximum tested range of use (m)	1	Several meters to few tens of metres (FAQ)	0.5 to 1	1.5	0.54	Up to 8.4 and 16.8 expected	2	7	11
Cold-start compatibility	N/A	N/A	YES		YES	YES	YES	YES	
Periodicity	27 s	N/A	0.5 s		8 s to 259 s	21 s to 2 h 20 min (controlled by MCU)	5 s to 18 s	33 s to 14 h 38 min (controlled by WPT)	6 s to 7 h 59 min (controlled by WPT)
Energy buffer	100 µF capacitor	200 µF tunable capacitor	Capacitor		2 470 µF capacitors	8 mF capacitor	1 mF capacitor	22 mF supercapacitor	2.2 mF supercapacitor
Consumption strategy	Simultaneous store and use	N/A	Simultaneous store and use		Store then use	Simultaneous store and use OR store then use	Store then use	Store then use	
Size (cm x cm x cm)	Not-fully implemented	7 x 5.2 x 0.9 (without antenna)	Not integrated		3 x 3 x 0.5	Not integrated	Not integrated	14 x 9 x 6	8 x 6 x 5

* Temperature measurements (that can be combined with humidity and/or strength measurements) are usually used during the curing phase in order to monitor the concrete maturity.

powered, and controlled, and part of a CPS that can automate the monitoring, is proposed here.

Thus, the proposed communicating reinforced concrete can be characterized as a nonintrinsic self-sensing and data storing reinforced concrete based on the use of an embedded fully WSN composed of buried SNs employing NDT methods. These SNs can use a large variety of sensors to measure various parameters of the reinforced concrete during its entire life, and can be considered as wide aggregates planned in the recipe, randomly located and physically inaccessible. The range of use of both the WPT and the wireless communication of the implemented WSN covers a relevant volume of reinforced concrete (that says at least from ten of meters in all the directions), and for long term, (that says for decades). Moreover, its use is automated and does not required human interventions or external equipment; it wirelessly connects the digital world through the Internet; the traceability, the data storage in the material, and the SHM are simultaneous ensured during all its life. Finally, its deployment is independent of the environment and of the targeted application.

B. Current Solutions for the Wireless Power Transfer of Wireless Sensor Networks

The proposed solution can easily be scalable to other applications and can also be considered as a WSN wirelessly powered.

Today there are few commercially available solutions to recharge the battery of devices through radiative WPT [120], [121]. Moreover, these are limited in terms of distance and of efficiency: it is more a question of increasing the discharge time of a device than really recharging it during its use.

Nevertheless, some academic research or few start-up companies deal with complete battery-free SNs wirelessly powered through radiative WPT and which use LPWANs or WPAN wireless communication technologies [101], [112], [122], [123], [124], [125], [126]. The latter are compared in Table III. Besides, these meet the requirements of the SWIPT paradigm, thanks to frequency and/or spatial multiplexing. Among these, few are dedicated to the SHM of civil infrastructures but are always deployed on the surface of existing

structures and could require the use of a vehicle, such as [101] and [112].

Finally, some works deal with the theoretical or experimental aspects of the radiative WPT through the reinforced concretes, and study especially the impact of the reinforcements [127], [128], [129], [130].

Thus, the proposed solution is only based on off-the-shelf components (excepted for the rectenna, for which no commercial solution is available); employs a unique antenna and a radio-frequency circulator both for the wireless communication and the WPT which take place in the same ISM frequency band; allows the implementation of a complete CPS from the measurement inside the reinforced concrete to the process and storage in the digital world *via* the Internet, and through the wireless communication; and is successfully deployed in a harsh environment, namely, the reinforced concrete which is a harsh medium of propagation for the electromagnetic waves. Regarding the range of use, this is mainly constrained by the WPT and not by the wireless communication, but it covers several meters, which is more than a major part of the published solution. Only one proposition provides higher theoretical ranges of use (16.8 m) but by using a commercially unavailable PMU [124]. Nevertheless, by optimizing the proposed solution, this range of use seems to be reachable. Because long periodicities are targeted (on a daily, weekly or monthly base) the "store then use" strategy with a cold start ability seems the most appropriate configuration for the targeted application. Furthermore, as long lifespans are wanted, the design provides as little components and complexity as possible in order to limit as much as possible the points of failure.

C. Areas of Improvement and Future Works

The proposed SNs are presented as true prove-of-concept. Nevertheless, these can be optimized both on hardware and on software.

First, each component of the electromagnetic energy harvester (antenna and rectifier), as well as their association (through the impedance matching network), can be improved, and tuned to be the most effective on the targeted frequencies and power densities [5], [131]. Moreover, the rectenna can be designed to be multiband or wideband to scavenge a larger part of the available electromagnetic spectrum, and can be placed in arrays to scavenge larger part of the available electromagnetic power. The frequency band(s) and the bandwidth(s) of a rectenna are imposed by the smallest overlap between those of the antenna and those of the rectifier, which is related to their impedance matching. The relevant parameters of a rectifier are, between others: its topology (e.g., shunt, in series, doubler, Dickson charge pump, etc.); its nonlinear rectifying element (e.g., diode, Schottky diode, tunnel diode, metal-insulator-metal diode, spin-diode, complementary metal–oxide semiconductor (CMOS) transistor, etc.); its frequency band(s); and its bandwidth(s). The relevant parameters of an antenna are, between others: its type (e.g., patch, dipole, etc.); its frequency band(s); its bandwidth(s); its polarization (linear, circular or elliptic); its gain in each frequency band(s); and its radiation pattern. Thus, the rectenna can be characterized regarding: its frequency band(s); its bandwidth(s); its minimum power density required; its efficiency; its output voltage and current; its optimal load; but also, its size and its weight. In fact, the size of the SN is correlated to the size of its antenna, which is closely related to the wavelength, and therefore, a tradeoff must be found between volume and performances (especially the radiation pattern and gain). Finally, the rectenna can be manufactured thanks to 3-D or inkjet printing, or additive techniques, and on various substrates (e.g., polyethylene terephthalate (PET), paper, textile, etc.), which can be flexible [5], [131].

The antenna must also be tuned to efficiently operate direct contact of the reinforced concrete both for the WPT and the wireless communication [47], [52].

In addition to the improvement of the rectenna and with the same aim of lengthening the range of use of the WPT, the minimum input power required by the data power subsystem must be minimized. This can be achieved by reducing the power required by the PMU (e.g., by using another one) and lost by the energy buffer and the dc-to-dc converter [57], [58], [59].

To shorten the duration of the first charge and recharge, in addition to optimizing the power management subsystem, the energy required by the data management subsystem must be reduced (e.g., by using lower power MicroControler Unit, transceiver, and sensor, or employing other solutions). Thus, first tests have been performed by using Bluetooth Low Energy wireless communication technology [with a QN9080 all-in-one module from NXP Semiconductors (Eindhoven, Netherlands)] rather than LoRaWAN [39]. The implemented SNs do not have the same level of maturity as the previous ones and use two antennas because two different ISM frequency bands are used. The Bluetooth Low Energy is configured in broadcaster/observer mode, and allows to reduce the energy needed by the data management subsystem, at the cost of a less resilient and shorter range wireless communication. This is highly impacted by the reinforced concrete. This implementation requires 1.16 mJ to be stored in a 100-μF EEEFK0J101P capacitor from Panasonic (Kadoma, Osaka, Japan). This allows a complete process with the initializations, the measurement, the formatting, and the four transmissions of a 19-bytes long advertising frame (whose only 3 bytes are dedicated to the data payload) on three different advertising channels for a transmission power of +0 dBm and a data rate of 1 Mb/s. In other words, 1.16 mJ stored is also 390 μJ per data byte, or 61.6 μJ per transmitted byte, or 7.7 μJ per transmitted bit. Consequently, another tradeoff between the reliability of the wireless communications and the energy consumption must be sought. The redundancy through the transmission of more frames on more channels allows to increase the reliability at the cost of more important energy needs.

The current sensors must also be optimized to be more accurate and to consume less power, and other sensors must be employed. In addition, the resistivity sensor must be improved by using an alternative current source to limit the polarization effect on the concrete, and configurations other than the Wenner could be implemented [24], [119].

In complement to the improvement of the rectenna, the overall efficient of the WPT system and its range of use can be increased by focusing the transmitted power on the SNs thanks to beamforming [62], [63], [64] or FDAs [65], [66] techniques, to waste as little power as possible, but also by employing more efficient waveforms [5], [64], [131], [132] or by using relays [133]. Finally, there are also solutions used to recover the energy due to the harmonics lost during the wireless data transmission [134].

With a different approach, alternative strategies of deployment of the SNs in the reinforced concrete can be discussed. It is possible: 1) to deploy only the sensor in the core of the concrete and the rest of the SN near or on the surface so the measurements are performed in the places defined as the most relevant and the SNs are accessible, thus replaceable and updatable; but also 2) to deploy the SN in the core of the concrete and the antenna near or on the surface so the measurements are performed in the places defined as the most relevant and the SNs are inaccessible but the constraints of the electromagnetic propagation through the reinforced concrete are released [19]. In these two cases, the use of wires between the different parts can create weaknesses in the reinforced concrete and an access on the surface is also an access point for the pollutants and other contaminants, such as the air and the water which can induce faster corrosion.

The last point of work is the packaging, which must allow to deploy the SNs directly in the reinforced concrete (no more in air cavities) and to make possible reliable measurements in it [86], [87], [94], [119], [135], [136].

Finally, it could be noted that the design and the implementation of this CPS were carried out simultaneously by considering the cybersecurity aspects (especially data integrity, confidentiality, and availability), through a security analysis, in particular by defining the main hypothesis of the attacks and its consequences, but also the countermeasures and the security solutions [137].

V. Conclusion

In the framework of the McBIM project, a CPS dedicated to the SHM of reinforced concrete is proposed through the design and implementation of a communicating reinforced concrete. This IIoT system allows to connect the physical and digital worlds through the Internet, by employing a WSN composed of CNs and SNs. The SNs are able to locally generate, format, and transmit measured physical data, and the CNs are able to locally gather, locally and/or remotely process, store, and exchange the collected data. The SNs, which are the core of this article, are generic being able to use sensors for measuring various relevant parameters for the SHM of reinforced concrete (e.g., the temperature, the relative humidity, the mechanical deformation, and the electrical resistivity). These are low-power, battery-free, able to cold-start, wirelessly energized, and remotely powered and controlled by a radiative WPT system part of the CNs. Moreover, these SNs are designed to be fully buried in the reinforced concrete.

The proposed CPS is based on, to the best of out knowledge, the first fully buried, fully wireless, and energy autonomous SNs, which is, in addition, able to estimate the corrosion rate by electrical resistivity measurement performed inside the reinforced concrete. This IIoT system can be easily scaled to other applications, with less restrictive medium (in terms of electromagnetic waves propagation) than the reinforced concrete. Experimental results demonstrated that the prototypes of the SNs have been omnidirectionally powered and controlled by a CN up to 11-m indoors. Higher ranges of use (in terms of WPT) could be achieved with some improvements in terms of rectenna sensitivity and efficiency. It must be noted that this is not the wireless communications—here based on the LoRaWAN technology (which can work over at least tens of meters from a reinforced concrete beam, and up to kilometers outdoors)—which limits the range of use, but the WPT, specifically in regards of the maximum EIRP allowed by the regional regulators according to the frequency band (here of +33 dBm, or +3 dB, or 2 W) and the rectenna efficiency. By simultaneously using the 868-MHz ISM frequency band for both the wireless communication and the WPT, the SNs meet the requirement of the SWIPT paradigm by using a unique antenna and a radio-frequency circulator. The SNs are considered physically inaccessible because buried in the reinforced concrete, and no data downlink is implemented between the CNs and the SNs. The periodicity of measurement and wireless communication are not defined by software nor hardware, this is through the WPT system and its power/energy downlink path that this periodicity is tuned by the CNs. Lower the energy to store and higher the power harvested, shorter the periodicity. Thus, a maximum periodicity between several hours and a few seconds can be achieved, respectively, for harvested electromagnetic powers (measured at the input of the radio-frequency rectifier) between −17 and +15 dBm.

Acknowledgment

The authors would like to thank all their French partners in the McBIM project: CRAN (Nancy, France), LIB (Dijon, France), and FINAO SAS/360SmartConnect (Trans-n-Provence, France); and in the OPTENLOC project: UWINLOC (Toulouse, France); but also Prof. Jean-Paul Balayssac from the Laboratory for Materials and Durability of Constructions (LMDC, Toulouse, France) and Prof. Florin Udrea, Dr. Andrea De Luca, and Dr. Ethan Gardner from the Centre for Advanced Photonics and Electronics (CAPE) of the University of Cambridge.

References

[1] F. Montori, L. Bedogni, M. Di Felice, and L. Bononi, "Machine-to-machine wireless communication technologies for the Internet of Things: Taxonomy, comparison and open issues," *Pervasive Mobile Comput.*, vol. 50, pp. 56–81, Oct. 2018.

[2] S. Zeadally and N. Jabeur, *Cyber-Physical System Design With Sensor Networking Technologies*, 1st ed. London, U.K.: Inst. Eng. Technol., 2016, p. 368.

[3] A. Čolaković and M. Hadžialić, "Internet of Things (IoT): A review of enabling technologies, challenges, and open research issues," *Comput. Netw.*, vol. 144, pp. 17–39, Oct. 2018.

[4] G. Peruzzi and A. Pozzebon, "A review of energy harvesting techniques for low power wide area networks (LPWANs)," *Energies*, vol. 13, no. 13, p. 3433, 2020.

[5] A. Georgiadis, A. Collado, and M. M. Tentzeris, *Energy Harvesting: Technologies, Systems, and Challenges*, 1st ed. Cambridge, U.K.: Cambridge Univ. Press, 2021, p. 208.

[6] *Commission Implementing Decision (EU) 2017/1483 of 8 August 2017 Amending Decision 2006/771/EC on Harmonisation of the Radio Spectrum for Use by Short-Range Devices and Repealing Decision 2006/804/EC*, Eur. Union, Washington, DC, USA, 2017.

[7] T. D. P. Perera, D. N. K. Jayakody, S. K. Sharma, S. Chatzinotas, and J. Li, "Simultaneous wireless information and power transfer (SWIPT): Recent advances and future challenges," *IEEE Commun. Surveys Tuts.*, vol. 20, no. 1, pp. 264–302, 1st Quart., 2018.

[8] C. R. Farrar and K. Worden, "An introduction to structural health monitoring," *Philos. Trans. Roy. Soc. A Math. Phys. Eng. Sci.*, vol. 365, no. 1851, pp. 303–315, 2007.

[9] J. H. Bungey, S. G. Millard, and M. G. Grantham, *Testing of Concrete in Structures*, 4th ed. Boca Taron, FL, USA: CRC Press, 2006, p. 353.

[10] S. K. Verma, S. S. Bhadauria, and S. Akhtar, "Review of nondestructive testing methods for condition monitoring of concrete structures," *J. Construct. Eng.*, vol. 2013, no. 2008, pp. 1–11, 2013.

[11] P. Kot, M. Muradov, M. Gkantou, G. S. Kamaris, K. Hashim, and D. Yeboah, "Recent advancements in non-destructive testing techniques for structural health monitoring," *Appl. Sci.*, vol. 11, no. 6, p. 2750, 2021.

[12] S. Tang, D. R. Shelden, C. M. Eastman, P. Pishdad-Bozorgi, and X. Gao, "A review of building information modeling (BIM) and the Internet of Things (IoT) devices integration: Present status and future trends," *Autom. Construct.*, vol. 101, pp. 127–139, May 2019.

[13] S. Kubler, W. Derigent, A. Thomas, and E. Rondeau, "Problem definition methodology for the 'communicating material' paradigm," *IFAC Proc. Vol.*, vol. 43, no. 4, pp. 198–203, 2010.

[14] "McBIM." Accessed: Apr. 20, 2023. [Online]. Available: https://mcbim.cran.univ-lorraine.fr/

[15] W. Derigent et al., "Materials communicating with the BIM: Results of the McBIM project," *IFAC-PapersOnLine*, vol. 55, no. 8, pp. 25–30, 2022.

[16] G. Loubet, "Autonomous wireless sensor networks for the implementation of communicating materials. Application to civil engineering industry," Ph.D. dissertation, Dept. Comput. Sci., INSA Toulouse, Toulouse, France, Sep. 2021.

[17] G. Loubet, A. Takacs, E. Gardner, A. De Luca, F. Udrea, and D. Dragomirescu, "LoRaWAN battery-free wireless sensors network designed for structural health monitoring in the construction domain," *Sensors*, vol. 19, no. 7, p. 1510, 2019.

[18] G. Loubet, A. Takacs, and D. Dragomirescu, "Implementation of a wireless sensor network designed to be embedded in reinforced concrete," in *Proc. 46th Annu. Conf. IEEE Ind. Electron. Soc. (IECON)*, 2020, pp. 2195–2200.

[19] S. S. Zhekov, O. Franek, and G. F. Pedersen, "Dielectric properties of common building materials for ultrawideband propagation studies [measurements corner]," *IEEE Antennas Propag. Mag.*, vol. 62, no. 1, pp. 72–81, Feb. 2020.

[20] S. Taheri, "A review on five key sensors for monitoring of concrete structures," *Construct. Build. Mater.*, vol. 204, pp. 492–509, Apr. 2019.

[21] A. De Luca, V. Pathirana, S. Z. Ali, D. Dragomirescu, and F. Udrea, "Experimental, analytical and numerical investigation of non-linearity of SOI diode temperature sensors at extreme temperatures," *Sensors Actuators A Phys.*, vol. 222, pp. 31–38, Feb. 2015.

[22] "Texas Instruments—HDC2010 low-power humidity and temperature digital sensors." Accessed: Apr. 20, 2023. [Online]. Available: https://www.ti.com/lit/ds/symlink/hdc2010.pdf

[23] "RS pro—Datasheet RS pro wire lead strain gauge 4mm, 120Ω." Accessed: Apr. 20, 2023. [Online]. Available: https://docs.rs-online.com/1c95/0900766b815882e1.pdf

[24] J. Badr, "Conception et validation d'un capteur noyéde résistivité électrique en vue du suivi des profils de teneur en eau dans les bétons," Ph.D. Dissertation, Université Paul Sabatier-Toulouse III, Toulouse, France, 2019.

[25] *IEEE Standard for Information Technology—Telecommunications and Information Exchange Between Systems—Local and Metropolitan Area Networks—Specific Requirements—Part 15.7: Short-Range Wireless Optical Communication Using Visible Light*, IEEE Standard 802.15.7, 2011.

[26] S. Siu, Q. Ji, W. Wu, G. Song, and Z. Ding, "Stress wave communication in concrete: I. Characterization of a smart aggregate based concrete channel," *Smart Mater. Struct.*, vol. 23, no. 12, 2014, Art. no. 125030.

[27] S. Siu, Q. Ji, X. Wu, G. Song, and Z. Ding, "Stress wave communication in concrete: II. Evaluation of low voltage concrete stress wave communications utilizing spectrally efficient modulation schemes with PZT transducers," *Smart Mater. Struct.*, vol. 23, no. 12, 2014, Art. no. 125031.

[28] G. Saulnier, H. Scarton, D. Shoudy, P. Das, and A. Gavens, "Ultrasonic through-wall communication (UTWC) system," U.S. Patent Appl. 12 443 878, 2010.

[29] J. S. Lee, Y. W. Su, and C. C. Shen, "A comparative study of wireless protocols: Bluetooth, UWB, ZigBee, and Wi-Fi," in *Proc. 33rd Annu. Conf. IEEE Ind. Electron. Soc. (IECON)*, 2007, pp. 46–51.

[30] *IEEE Standard for Information Technology—Telecommunications and Information Exchange Between Systems—Local and Metropolitan Area Networks—Specific Requirements—Part 15.1: Wireless Medium Access Control (MAC) and Physical Layer (PHY) Specifications for Wireless Personal Area Networks (WPANs)*, IEEE Standard 802.15.1, 2005.

[31] *IEEE Standard for Information Technology—Telecommunications and Information Exchange Between Systems—Local and Metropolitan Area Networks—Specific Requirements—Part 15.4: Wireless Medium Access Control (MAC) and Physical Layer (PHY) Specifications for Low-Rate Wireless Personal Area Networks (WPANs)*, IEEE Standard 802.15.4, 2006.

[32] *IEEE Standard for Local and Metropolitan Area Networks—Part 15.4: Low-Rate Wireless Personal Area Networks (LR-WPANs)*, IEEE Standard 802.15.4, 2011.

[33] U. Raza, P. Kulkarni, and M. Sooriyabandara, "Low power wide area networks: An overview," *IEEE Commun. Surveys Tuts.*, vol. 19, no. 2, pp. 855–873, 2nd Quart., 2017.

[34] *LoRaWAN 1.0.3 Specification*, LoRa Alliance Technical Committee, San Ramon, CA, USA, 2018.

[35] *International Organization for Standardization/International Electrotechnical Commission. Information Technology—Radio Frequency Identification for Item Management*, ISO/IEC Standard 18000, 2015.

[36] *IEEE Standard for Information Technology—Telecommunications and Information Exchange Between Systems—Local and Metropolitan Area Networks—Specific Requirements—Part 15.3: Wireless Medium Access Control (MAC) and Physical Layer (PHY) Specifications for High Rate Wireless Personal Area Networks (WPAN)*, IEEE Standard 802.15.3, 2003.

[37] *IEEE Standard for High Data-Rate Wireless Multimedia Networks*, IEEE Standard 802.15.3, 2016.

[38] *IEEE Standard for Long Wavelength Wireless Network Protocol*, IEEE Standard 1902.1, 2009.

[39] A. Sidibe, G. Loubet, A. Takacs, and D. Dragomirescu, "A multifunctional battery-free Bluetooth low energy wireless sensor node remotely powered by electromagnetic wireless power transfer in far-field," *Sensors*, vol. 22, no. 11, p. 4054, 2022.

[40] "Murata—Sub-G module data sheet." Accessed: Apr. 20, 2023. [Online]. Available: https://wireless.murata.com/pub/RFM/data/type_abz.pdf

[41] "Semtech. LoRa—SX1276/77/78/79." Accessed: Apr. 20, 2023. [Online]. Available: https://www.semtech.com/products/wireless-rf/lora-transceivers/SX1276

[42] "STMicroelectronics. B-L072Z-LRWAN1." Accessed: Apr. 20, 2023. [Online]. Available: https://www.st.com/en/evaluation-tools/b-l072z-lrwan1.html

[43] J. W. Matiko, N. J. Grabham, S. P. Beeby, and M. J. Tudor, "Review of the application of energy harvesting in buildings," *Meas. Sci. Technol.*, vol. 25, no. 1, 2013, Art. no. 12002.

[44] X. Gu, L. Grauwin, D. Dousset, S. Hemour, and K. Wu, "Dynamic ambient RF energy density measurements of Montreal for battery-free IoT sensor network planning," *IEEE Internet Things J.*, vol. 8, no. 17, pp. 13209–13221, Sep. 2021.

[45] "Aerotek Co., LTD.—Coaxial circulators/isolators." Accessed: Apr. 20, 2023. [Online]. Available: http://www.aerotek.co.th/classic/coaxstd.php

[46] A. Sidibe, A. Takacs, G. Loubet, and D. Dragomirescu, "Compact antenna in 3D configuration for rectenna wireless power transfer applications," *Sensors*, vol. 21, no. 9, p. 3193, 2021.

[47] K. M. Shams, M. Ali, and A. M. Miah, "Characteristics of an embedded microstrip patch antenna for wireless infrastructure health monitoring," in *Proc. IEEE Antennas Propag. Soc. Int. Symp.*, 2006, pp. 3643–3646.

[48] M. F. Rad and L. Shafai, "Embedded microstrip patch antenna for structural health monitoring applications," in *Proc. IEEE Antennas Propag. Soc. Int. Symp.*, 2008, pp. 1–4.

[49] X. Jin and M. Ali, "Embedded antennas in dry and saturated concrete for application in wireless sensors," *Progr. Electromagn. Res.*, vol. 102, pp. 197–211, Feb. 2012.

[50] S. H. Jeong and H. W. Son, "UHF RFID tag antenna for embedded use in a concrete floor," *IEEE Antennas Wireless Propag. Lett.*, vol. 10, pp. 1158–1161, 2011.

[51] R. Salama and S. Kharkovsky, "An embeddable microwave patch antenna module for civil engineering applications," in *Proc. IEEE Int. Instrum. Meas. Technol. Conf. (I2MTC)*, 2013, pp. 27–30.

[52] G. Castorina, L. Di Donato, A. F. Morabito, T. Isernia, and G. Sorbello, "Analysis and design of a concrete embedded antenna for wireless monitoring applications [antenna applications corner]," *IEEE Antennas Propag. Mag.*, vol. 58, no. 6, pp. 76–93, Feb. 2016.

[53] A. Sidibe, G. Loubet, A. Takacs, and D. Dragomirescu, "Energy harvesting for battery-free wireless sensors network embedded in a reinforced concrete beam," in *Proc. 50th Eur. Microw. Conf. (EuMC)*, 2021, pp. 702–705.

[54] "Skyworks—Surface-mount mixer and detector Schottky diodes." Accessed: Apr. 20, 2023. [Online]. Available: https://www.skyworksinc.com/-/media/SkyWorks/Documents/Products/201-300/Surface_Mount_Schottky_Diodes_200041AG.pdf

[55] "Texas Instruments—BQ25504." Accessed: Apr. 20, 2023. [Online]. Available: https://www.ti.com/product/BQ5504

[56] "Texas Instruments—TPS6303x high efficiency single inductor buck-boost converter." Accessed: Apr. 20, 2023. [Online]. Available: https://www.ti.com/lit/ds/symlink/tps63030.pdf

[57] "Texas Instruments—BQ25505." Accessed: Apr. 20, 2023. [Online]. Available: https://www.ti.com/product/BQ25505

[58] "Texas Instruments—BQ225570." Accessed: Apr. 20, 2023. [Online]. Available: https://www.ti.com/product/BQ25570

[59] "e-peas semiconductors—AEM30940—datasheet." Accessed: Apr. 20, 2023. [Online]. Available: https://e-peas.com/wp-content/uploads/2021/03/e-peas-AEM30940-datasheet-RF-Vibration-energy-harvesting.pdf

[60] "AVX—BestCap." Accessed: Apr. 20, 2023. [Online]. Available: https://catalogs.avx.com/BestCap.pdf

[61] "Panasonic—Aluminum electrolyic capacitor." Accessed:. Apr. 20, 2023. [Online]. Available: https://industrial.panasonic.com/cdbs/www-data/pdf/RDE0000/ABA0000C1190.pdf

[62] D. Belo, D. C. Ribeiro, P. Pinho, and N. B. Carvalho, "A selective, tracking, and power adaptive far-field wireless power transfer system," *IEEE Trans. Microw. Theory Techn.*, vol. 67, no. 9, pp. 3856–3866, Sep. 2019.

[63] D. Masotti, M. Shanawani, and A. Costanzo, "Smart beamforming techniques for 'on demand' WPT," in *Wireless Power Transmission for Sustainable Electronics*, Hoboken, NJ, USA: Wiley, 2020, pp. 57–84.

[64] J. Kim and B. Clerckx, "Range expansion for wireless power transfer using joint beamforming and waveform architecture: An experimental study in indoor environment," *IEEE Wireless Commun. Lett.*, vol. 10, no. 6, pp. 1237–1241, Jun. 2021.

[65] W. Q. Wang, "Retrodirective frequency diverse array focusing for wireless information and power transfer," *IEEE J. Sel. Areas Commun.*, vol. 37, no. 1, pp. 61–73, Jan. 2019.

[66] E. Fazzini, A. Costanzo, and D. Masotti, "Range selective power focusing with time-controlled bi-dimensional frequency diverse arrays," in *Proc. IEEE Wireless Power Transfer Conf. (WPTC)*, 2021, pp. 1–4.

[67] S. Kamila, "Introduction, classification and applications of smart materials: An overview," *Amer. J. Appl. Sci.*, vol. 10, no. 8, p. 876, 2013.

[68] B. Han, L. Zhang, and J. Ou, *Smart and Multifunctional Concrete Toward Sustainable Infrastructures*. Singapore: Springer, 2017, p. 409.

[69] N. Makul, "Advanced smart concrete—A review of current progress, benefits and challenges," *J. Clean. Prod.*, vol. 274, Nov. 2020, Art. no. 122899.

[70] B. Han, S. Ding, and X. Yu, "Intrinsic self-sensing concrete and structures: A review," *Measurement*, vol. 59, pp. 110–128, Jan. 2015.

[71] Z. Tian, Y. Li, J. Zheng, and S. Wang, "A state-of-the-art on self-sensing concrete: Materials, fabrication and properties," *Composites B Eng.*, vol. 177, Nov. 2019, Art. no. 107437.

[72] G. Kaklauskas, A. Sokolov, R. Ramanauskas, and R. Jakubovskis, "Reinforcement strains in reinforced concrete tensile members recorded by strain gauges and FBG sensors: experimental and numerical analysis," *Sensors*, vol. 19, no. 1, p. 200, 2019.

[73] A. Deraemaeker and C. Dumoulin, "Embedding ultrasonic transducers in concrete: A lifelong monitoring technology," *Construct. Build. Mater.*, vol. 194, pp. 42–50, Jan. 2019.

[74] G. Song, Y. L. Mo, K. Otero, and H. Gu, "Health monitoring and rehabilitation of a concrete structure using intelligent materials," *Smart Mater. Struct.*, vol. 15, no. 2, p. 309, 2006.

[75] N. Muto et al., "Hybrid composites with self-diagnosing function for preventing fatal fracture," *Composites Sci. Technol.*, vol. 61, no. 6, pp. 875–883, 2001.

[76] A. Downey, A. D'Alessandro, F. Ubertini, and S. Laflamme, "Automated crack detection in conductive smart-concrete structures using a resistor mesh model," *Meas. Sci. Technol.*, vol. 29, no. 3, 2018, Art. no. 35107.

[77] "Doka." Accessed: Apr. 20, 2023. [Online]. Available: https://www.doka.com/

[78] "Concrefy." Accessed: Apr. 20, 2023. [Online]. Available: https://www.concrefy.com/

[79] "360 SmartConnect." Accessed: Apr. 20, 2023. [Online]. Available: https://www.360sc.io/?lang=en

[80] "idencia—Connected concrete." Accessed: Apr. 20, 2023. [Online]. Available: http://www.idencia.com/connected-concrete

[81] J. Zhang, G. Y. Tian, A. M. Marindra, A. I. Sunny, and A. B. Zhao, "A review of passive RFID tag antenna-based sensors and systems for structural health monitoring applications," *Sensors*, vol. 17, no. 2, p. 265, 2017.

[82] *Review of Current State of Radio Frequency Identification (RFID) Technology, Its Use and Potential Future Use in Construction*, E. R. A. Build, London, U.K., 2006.

[83] N. Li and B. Becerik-Gerber, "Life-cycle approach for implementing RFID technology in construction: Learning from academic and industry use cases," *J. Construct. Eng. Manag.*, vol. 137, no. 12, pp. 1089–1098, 2011.

[84] J. Ikonen, A. Knutas, H. Hämäläinen, M. Ihonen, J. Porras, and T. Kallonen, "Use of embedded RFID tags in concrete element supply chains," *J. Inf. Technol. Construct.*, vol. 18, no. 7, pp. 119–147, 2013.

[85] E. Valero and A. Adán, "Integration of RFID with other technologies in construction," *Measurement*, vol. 94, pp. 614–620, Dec. 2016.

[86] S. Johann, C. Strangfeld, M. Müller, B. Mieller, and M. Bartholmai, "RFID sensor systems embedded in concrete—Requirements for long–term operation," *Mater. Today Proc.*, vol. 4, no. 5, pp. 5827–5832, 2017.

[87] S. G. N. Murthy, "Batteryless wireless RFID based embedded sensors for long term monitoring of reinforced concrete structures," in *Proc. Int. Symp. Non-Destructive Test. Civil Eng. (NDT-CE)*, 2015, pp. 15–17.

[88] X. Yi, C. Cho, J. Cooper, Y. Wang, M. M. Tentzeris, and R. T. Leon, "Passive wireless antenna sensor for strain and crack sensing—Electromagnetic modeling, simulation, and testing," *Smart Mater. Struct.*, vol. 22, no. 8, 2013, Art. no. 85009.

[89] M. M. Andringa, D. P. Neikirk, N. P. Dickerson, and S. L. Wood, "Unpowered wireless corrosion sensor for steel reinforced concrete," in *Proc. IEEE Sensors*, 2005, p. 4.

[90] B. Ozbey, V. B. Erturk, H. V. Demir, A. Altintas, and O. Kurc, "A wireless passive sensing system for displacement/strain measurement in reinforced concrete members," *Sensors*, vol. 16, no. 4, p. 496, 2016.

[91] B. L. Grisso, L. A. Martin, and D. J. Inman, "A wireless active sensing system for impedance-based structural health monitoring," in *Proc. 23rd Int. Modal Anal. Conf. (IMAC)*, 2005, pp. 1–8.

[92] W. Quinn, P. Angove, J. Buckley, J. Barrett, and G. Kelly, "Design and performance analysis of an embedded wireless sensor for monitoring concrete curing and structural health," *J. Civil Struct. Health Monitor.*, vol. 1, no. 1, pp. 47–59, 2011.

[93] M. Ceriotti et al., "Monitoring heritage buildings with wireless sensor networks: The Torre Aquila deployment," in *Proc. Int. Conf. Inf. Process. Sensor Netw.*, 2009, pp. 277–288.

[94] C. Y. Chang and S. S. Hung, "Implementing RFIC and sensor technology to measure temperature and humidity inside concrete structures," *Construct. Build. Mater.*, vol. 26, no. 1, pp. 628–637, 2012.

[95] A. B. Noel, A. Abdaoui, T. Elfouly, M. H. Ahmed, A. Badawy, and M. S. Shehata, "Structural health monitoring using wireless sensor networks: A comprehensive survey," *IEEE Commun. Surveys Tuts.*, vol. 19, no. 3, pp. 1403–1423, 3rd Quart., 2017.

[96] M. Z. A. Bhuiyan, J. Wu, G. Wang, J. Cao, W. Jiang, and M. Atiquzzaman, "Towards cyber-physical systems design for structural health monitoring: Hurdles and opportunities," *ACM Trans. Cyber Phys. Syst.*, vol. 1, no. 4, pp. 1–26, 2017.

[97] L. Gallucci et al., "An embedded wireless sensor network with wireless power transfer capability for the structural health monitoring of reinforced concrete structures," *Sensors*, vol. 17, no. 11, p. 2566, 2017.

[98] L. Angrisani et al., "An innovative embedded wireless sensor network system for the structural health monitoring of RC structures," in *Proc. RTSI 3rd IEEE Int. Forum Res. Technol. Soc. Ind.*, 2017, pp. 1–4.

[99] D. Bosma and P. Lindeman, "Autonomous battery less sensor for IoT applications in smart buildings: Low-power energy conversion and storage for RF energy harvesting," M.S. Thesis, School Comput., Delft Univ. Technol., Delft, The Netherlands, 2018.

[100] M. Abdulkarem, K. Samsudin, F. Z. Rokhani, and M. F. A. Rasid, "Wireless sensor network for structural health monitoring: A contemporary review of technologies, challenges, and future direction," *Struct. Health Monitor.*, vol. 19, no. 3, pp. 693–735, 2020.

[101] K. M. Farinholt, G. Park, and C. R. Farrar, "RF energy transmission for a low-power wireless impedance sensor node," *IEEE Sensors J.*, vol. 9, no. 7, pp. 793–800, Jul. 2009.

[102] "CAPTAE et le monitoring des structures." Accessed: Apr. 20, 2023. [Online]. Available: https://lerm.fr/instruments/captae/captae/

[103] "TELEMAC—Leading supplier of geotechnical & structural instrumentation." Accessed: Apr. 20, 2023. [Online]. Available: https://telemac.fr/en/

[104] "CEMENTYS—Surveille vos infrastructures." Accessed: Apr. 20, 2023. [Online]. Available: https://cementys.com/fr/

[105] "Itmsol instrumentation & monitoring." Accessed Apr. 20, 2023. [Online]. Available: https://www.itmsol.fr/

[106] "WAKE—Powerful wireless concrete temperature monitoring and reporting." Accessed: Apr. 20, 2023. [Online]. Available: https://www.wakeinc.com/

[107] "GIATEC—Revolutionizing concrete testing." Accessed: Apr. 20, 2023. [Online]. Available: https://www.giatecscientific.com/

[108] "LumiCON—Concrete sensors." Accessed: Apr. 20, 2023. [Online]. Available: https://lumicon.io/concrete-sensors/

[109] "HILTI—Concrete sensors." Accessed: Apr. 20, 2023. [Online]. Available: https://www.hilti.com/content/hilti/W1/US/en/services/tool-services/internet-of-things/concrete-sensors.html

[110] "Sensohive—Wireless sensors and IoT solutions." Accessed: Apr. 20, 2023. [Online]. Available: https://sensohive.com/

[111] "Maturix." Accessed: Apr. 20, 2023. [Online]. Available: https://maturix.com/

[112] "GreenWake technologies—Remote powering of sensors—No wires, no batteries, no worries." Accessed: Apr. 20, 2023. [Online]. Available: http://gnw-tech.com/home.htm

[113] T. Polonelli, D. Brunelli, M. Guermandi, and L. Benini, "An accurate low-cost Crackmeter with LoRaWAN communication and energy harvesting capability," in *Proc. 23rd IEEE Int. Conf. Emerg. Technol. Factory Autom. (ETFA)*, vol. 1, 2018, pp. 671–676.

[114] P. Boccadoro, B. Montaruli, and L. A. Grieco, "Quakesense, a LoRa-compliant earthquake monitoring open system," in *Proc. 23rd IEEE/ACM Int. Symp. Distrib. Simulat. Real Time Appl. (DS-RT)*, 2019, pp. 1–8.

[115] F. Orfei, C. B. Mezzetti, and F. Cottone, "Vibrations powered LoRa sensor: An electromechanical energy harvester working on a real bridge," in *Proc. IEEE SENSORS*, 2016, pp. 1–3.

[116] "GIATEC—iCOR wireless NDT corrosion detection." Accessed: Apr. 20, 2023. [Online]. Available: https://www.giatecscientific.com/products/concrete-ndt-devices/icor-rebar-corrosion-rate/

[117] "Screening eagle—Proceq resipod." Accessed: Apr. 20, 2023. [Online]. Available: https://www.screeningeagle.com/en/products/resipod

[118] "CEMENTYS—CorroVolta corrosion sensor." Accessed: Apr. 20, 2023. [Online]. Available: https://cementys.com/en/corrosion-sensor-monitoring-corrovolta/

[119] D. M. Corva, S. S. Hosseini, F. Collins, S. D. Adams, W. P. Gates, and A. Z. Kouzani, "Miniature resistance measurement device for structural health monitoring of reinforced concrete infrastructure," *Sensors*, vol. 20, no. 15, p. 4313, 2020.

[120] "Powercast—Wireless power for a wireless world." Accessed: Apr. 20, 2023. [Online]. Available: https://www.powercastco.com/

[121] "Ossia." Accessed: Apr. 20, 2023. [Online]. Available: https://www.ossia.com/

[122] J. Janhunen, K. Mikhaylov, and J. Petäjäjärvi, "Experimental RF-signal based wireless energy transmission," in *Proc. IEEE Eur. Conf. Netw. Commun. (EuCNC)*, 2017, pp. 1–6.

[123] G. Paolini, D. Masotti, M. Guermandi, M. Shanawani, L. Benini, and A. Costanzo, "An ambient-insensitive battery-less wireless node for simultaneous powering and communication," in *Proc. 50th IEEE Eur. Microw. Conf. (EuMC)*, 2021, pp. 522–525.

[124] M. Pizzotti et al., "A long-distance RF-powered sensor node with adaptive power management for IoT applications," *Sensors*, vol. 17, no. 8, p. 1732, 2017.

[125] R. La Rosa, C. Trigona, G. Zoppi, C. A. Di Carlo, L. Di Donato, and G. Sorbello, "RF energy scavenger for battery-free wireless sensor nodes," in *Proc. IEEE Int. Instrum. Meas. Technol. Conf. (I2MTCT)*, 2018, pp. 1–5.

[126] J. Janhunen, K. Mikhaylov, J. Petäjäjärvi, and M. Sonkki, "Wireless energy transfer powered wireless sensor node for green IoT: Design, implementation and evaluation," *Sensors*, vol. 19, no. 1, p. 90, 2019.

[127] K. M. Shams and M. Ali, "Wireless power transfer to a buried sensor in concrete," *IEEE Sensors J.*, vol. 7, no. 12, pp. 1573–1577, Dec. 2007.

[128] S. Jiang and S. V. Georgakopoulos, "Optimum wireless powering of sensors embedded in concrete," *IEEE Trans. Antennas Propag.*, vol. 60, no. 2, pp. 1106–1113, Feb. 2012.

[129] S. Jiang, S. V. Georgakopoulos, and H. Jin, "Effects of periodic reinforced-concrete structures on power transmission," in *Proc. IEEE Int. Conf. RFID*, 2012, pp. 16–23.

[130] S. Jiang, S. V. Georgakopoulos, and O. Jonah, "Power transmission for sensors embedded in reinforced concrete structures," in *Proc. IEEE Int. Symp. Antennas Propag.*, 2012, pp. 1–2.

[131] N. B. Carvalho et al., "Wireless power transfer: R&D activities within Europe," *IEEE Trans. Microw. Theory Techn.*, vol. 62, no. 4, pp. 1031–1045, Apr. 2014.

[132] A. Boaventura, D. Belo, R. Fernandes, A. Collado, A. Georgiadis, and N. B. Carvalho, "Boosting the efficiency: Unconventional waveform design for efficient wireless power transfer," *IEEE Microw. Mag.*, vol. 16, no. 3, pp. 87–96, Apr. 2015.

[133] M. A. Hossain, R. M. Noor, K. L. A. Yau, I. Ahmedy, and S. S. Anjum, "A survey on simultaneous wireless information and power transfer with cooperative relay and future challenges," *IEEE Access*, vol. 7, pp. 19166–19198, 2019.

[134] D. Allane, G. A. Vera, Y. Duroc, R. Touhami, and S. Tedjini, "Harmonic power harvesting system for passive RFID sensor tags," *IEEE Trans. Microw. Theory Techn.*, vol. 64, no. 7, pp. 2347–2356, Jul. 2016.

[135] N. Barroca, L. M. Borges, F. J. Velez, F. Monteiro, M. Gorski, and J. Castro-Gomes, "Wireless sensor networks for temperature and humidity monitoring within concrete structures," *Construct. Build. Mater.*, vol. 40, pp. 1156–1166, Mar. 2013.

[136] E. Fraile-Garcia, J. Ferreiro-Cabello, E. M. De Pison Ascacibar, J. F. Ceniceros, and A. V. P. Espinoza, "Implementing a technically and economically viable system for recording data inside concrete," *Construct. Build. Mater.*, vol. 157, pp. 860–872, Dec. 2017.

[137] G. Loubet, E. Alata, A. Takacs, and D. Dragomirescu, "A survey on the security challenges of low-power wireless communication protocols for communicating concrete in civil engineerings," *Sensors*, vol. 23, no. 4, p. 1849, 2023.

Gaël Loubet (Member, IEEE) was born in Toulouse, France, in 1994. He received the Engineer Diploma degree in automatic control and electronics and the Ph.D. degree in micro- and nano-systems from the National Institute of Applied Sciences of Toulouse (INSA Toulouse), Toulouse, in 2017 and 2021, respectively.

From 2021 to 2022, he was a Teaching and Research Associate with INSA Toulouse and LAAS-CNRS. Since 2022, he has been an Associate Professor with INSA Toulouse and LAAS-CNRS. He has authored 20 articles in refereed journals or communications in international conferences. His research interests include electromagnetic wireless power transfer, wireless communication for the Internet of Things applications, and wireless sensor networks for cyber–physical systems implementation and structural health monitoring applications.

Alassane Sidibe (Member, IEEE) was born in Dakar, Senegal, in 1994. He received the M.Sc. degree in electronics of embedded system and telecommunications from the University Paul Sabatier of Toulouse, Toulouse, France, in 2018. He is currently pursuing the Ph.D. degree in communication engineering with the French Company UWINLOC, Toulouse.

He has authored and coauthored 13 research papers in IEEE international conference proceedings and three articles in refereed journals. His current research interests include wireless power transmission and energy harvesting for battery-free tags, wireless sensor network, and antenna design on flexible materials.

Philippe Herail was born in Vernon, France, in 1998. He received the Engineer Diploma degree in computer science and networks from the National Institute of Applied Sciences, Toulouse, France, in 2020, where he is currently pursuing the Ph.D. degree in computer science and robotics.

His current research interests include automated learning of planning models for autonomous agents and data-efficient machine learning.

Alexandru Takacs (Member, IEEE) was born in Simleu Silvaniei, Romania, in 1975. He received the Engineer Diploma degree in electronic engineering from the Military Technical Academy, Bucharest, Romania, in 1999, and the master's and Ph.D. degrees in microwave and optical communications from the National Polytechnic Institute of Toulouse, Toulouse, France, in 2000 and 2004, respectively.

From 2004 to 2007, he was a Lecturer with the Military Technical Academy, and an Associate Researcher with the Microtechnology Institute, Bucharest. From 2008 to 2010, he occupied a postdoctoral position with LAAS-CNRS, Toulouse. In 2011, he was a Research and Development RF Engineer with Continental Automotive SAS France, Toulouse, where he was in charge of antenna design and automotive electromagnetic simulation. Since 2012, he has been an Associate Professor with the University Paul Sabatier, Toulouse, where he performs research within LAAS–CNRS. He has authored or coauthored five international patents, 37 papers in refereed journals, one book, one book chapter, and over 110 communications in international symposium proceedings. His research interests include the design of microwave and RF circuits, energy harvesting and wireless power transfer, battery-free wireless sensors, small antenna design, electromagnetic simulation techniques, and optimization methods.

Daniela Dragomirescu (Senior Member, IEEE) received the engineering degree (*magna cum laude*) from the Polytechnic University of Bucarest, Bucharest, Romania, in 1996, the M.Sc. degree in circuits design from the University Paul Sabatier, Toulouse, France, in 1997, and the Ph.D. degree (*magna cum laude*) from the University of Toulouse, Toulouse, in 2001.

She is a Professor with the National Institute of Applied Sciences of Toulouse (INSA Toulouse), Toulouse, and has been the Deputy Director of LAAS-CNRS laboratory since January 2022. She was the French Government Fellow of the Churchill College, University of Cambridge, Cambridge, U.K., in 2014. She was the Dean of the Electrical and Computer Engineering Department, INSA Toulouse from June 2017 to September 2020. She published more than 90 papers in journals and conference proceedings, two patents, and authored seven academic courses. She is conducting research in the area of micro and nano systems for wireless communications with a special focus on wireless sensor networks.

Prof. Dragomirescu is the IEEE SOLID STATES CIRCUITS French Chapter Chair.